

Effectiveness of fluid-viscous dampers for improved seismic performance of inter-storey isolated buildings



Yanhui Liu^a, Jinbiao Wu^a, Marco Donà^{b,*}

^a Earthquake Engineering Research & Test Center (EERTC), University of Guangzhou, China

^b Department of Civil, Architectural and Environmental Engineering (ICEA), University of Padova, Italy

ARTICLE INFO

Keywords:

Supplementary viscous damping
Inter-storey isolation
Multi-objective optimal design
Genetic algorithm
Fluid viscous damper (FVD)
Lead rubber bearing (LRB)

ABSTRACT

The use of fluid viscous dampers (FVDs) together with isolators, frequent in near-fault buildings, is effective in reducing displacements of the isolation layer. Such a hybrid system is also beneficial in the case of inter-storey isolation with the aim of limiting P- Δ effects. However, previous research on base isolation shows that this additional damping may also be detrimental, as inter-storey drifts and floor accelerations may increase.

This paper analyses the effectiveness of FVDs for enhanced seismic performance of systems with inter-storey isolation. A seven-floor building, with natural and lead rubber bearings between the second and third levels, was used as a case study, and a multi-objective optimal design was performed to identify the best damper parameters. In particular, time-history analyses with various natural records were carried out and two competing objectives were examined: minimisation of the deflection of the isolation layer and minimisation of the total drift of the superstructure.

The results show not only the effectiveness of optimal FVDs but also the fact that their optimal linearity degree depends to a great extent on the non-linear seismic response of the structure, i.e., on the type of earthquake. The simplest design approach, consisting of applying an optimization algorithm for each design accelerogram, did not seem, in this case, to be sufficient to identify the best overall design solution. The design consequences of these findings are discussed.

1. Introduction

Inter-storey seismic isolation has attracted increasing interest in recent years, particularly in densely populated areas, as an alternative mitigation strategy to base isolation for both new and existing buildings. As the name suggests, the isolation system is incorporated between storeys rather than at the base of the structure, in view of architectural concerns, feasibility of construction, and performance benefits. Although base isolation for multi-storey buildings is a well-known technique applied worldwide, it may sometimes clash with substantial economic and technical problems, which may limit its application.

In particular, installing base isolation is straightforward for new buildings, but becomes complicated and expensive for existing ones, since excavation and temporary support works are required. Instead, the installation of inter-storey isolation is relatively simple and generally less expensive and disruption-free. It also allows extra floors to be constructed on an existing building (if its vertical capacity allows this) without increasing the total base shear demand, and thus represents an

innovative and realistic retrofitting approach [1,2].

Firstly, base isolation is not as effective for medium/high-rise buildings as inter-storey isolation, because of the flexibility and bending-type behaviour of the latter [3]. Secondly, storey isolation can greatly increase design flexibility in high-rise and multipurpose buildings, by separating them into two independent structural parts which can be designed with different shapes, materials and functions, thus allowing them to become unique architectural features [4]. Examples of this application to irregular high-rise buildings are the Iidabashi First Building [4] and the Shiodome Sumitomo Building [5] in Japan, two multipurpose buildings having substructure and superstructure with different structural shape. In China, this technique was used to isolate 50 buildings (seven- or nine-storey RC frames) in Beijing, built on top of a two-storey platform covering a very large ($\sim 3 \text{ km}^2$) railway area [6]. Built relatively recently, in the National Taiwan University campus, the Civil Engineering Research Building is a nine-storey pre-cast RC structure with an inter-storey isolation system installed between the second and third floors, which also includes viscous dampers [7]. Lastly, moving the isolation layer to the upper storeys reduces the need for a

* Corresponding author at: Via Marzolo 9, 35131 Padova, Italy.
E-mail address: marco.dona@dicea.unipd.it (M. Donà).

seismic gap, which is necessary to accommodate the expected displacement of isolators, but also expensive and sometimes impractical in densely-built urban areas.

This isolation strategy, which can be achieved by inserting isolators inside the columns of a chosen storey (especially for retrofitting applications) or between RC slabs (i.e., the top and base of the substructure and superstructure, respectively), substantially converts the masses above the isolation layer into tuned masses, retaining their structural functions in addition to the control function; in other words, the principle of operation may be appropriately described as a non-conventional tuned mass damper (TMD) with a large mass ratio [8].

Fluid viscous dampers (FVDs) and other damping devices are often used together with isolators. Their primary function is to reduce the seismic demand which, in some cases, requires isolation devices of considerable size and cost to avoid their buckling or rupture. This is particularly true in the case of near-fault (NF) ground motions, characterized by intense long-period pulses of motion, for which several authors have shown the need for additional damping [9–11]. However, such hybrid systems are also very effective in the case of inter-storey isolation, reducing P- Δ effects due to drift between the structural parts separated by the isolation layer.

Kelly [12] questioned the usefulness of this supplementary damping on the basis of analytical treatment of a linear two degrees-of-freedom (DOF) base-isolated structure. He concluded that it reduced the efficiency of the isolation system by exciting higher modes, leading to higher floor accelerations and inter-storey drift. This was disputed by Hall [13] who, through time-history analyses of a 2-DOF linear system, demonstrated that supplementary damping can reduce the displacement demand of the isolation system and may also reduce drift. Further studies demonstrating these advantages of added linear viscous damping were performed by other authors, such as: Hall and Ryan [14], who carried out response history analyses on high damping rubber bearings and linear viscous dampers; Jangid and Kelly [15], who studied the effects of isolation damping on the performance of various isolation systems under near-fault motion; Alhan and Gavin [16], who performed time and frequency domain analyses on an eight-storey structural model, isolated with both linear viscously damped and non-linear yielding hysteretic systems; Politopoulos [17] who, again investigating a base-isolated 2-DOF system, confirmed the conclusions of Hall [13], and also showed how additional damping can reduce floor spectra values in the vicinity of the first mode - at the expense, however, of a possible increase of the same values near higher modal frequencies. Providakis [18,19] and Fathi et al. [20] have recently provided other numerical studies on supplementary linear viscous damping; Providakis studied two realistic base-isolated RC buildings, examining both lead rubber bearings (LRB) and single friction pendulum (FPS) isolators, and Fathi et al. investigated ideal moment-resisting steel frames, base-isolated with LRB devices. Some of their conclusions were similar: for instance, an increase in the damping ratio reduces the base displacement for both near-fault (NF) and far-fault (FF) earthquakes, while sometimes amplifying floor accelerations. However, results regarding inter-storey drift are conflicting; according to Providakis [18,19], if the damping ratio increases, drift decreases in the case of NF and increases in that of FF, which may be the result of 'too much damping' in the weaker FF motions.

Some interesting applications of FVDs in isolation systems, in the USA and particularly in California, are reported in Wolff et al. [21]. These authors observed that, despite the now widespread use of non-linear FVDs, the application of FVDs in isolation systems has progressed toward using linear dampers. Another example in which linear FVDs were placed in a storey isolation system is the previously mentioned building in the National Taiwan University campus [7].

A non-linear FVD (i.e., with damping exponent α of less than 1) dissipates more energy per cycle than a linear one (i.e., with α approximately equal to 1), considering the same maximum damping force and displacement amplitude. It also provides a safeguard by limiting

the transmission of damping force at high velocities beyond the design value [22,23]. Instead, in the case of sinusoidal or similar motions, a linear damper allows containment of the total force at maximum displacement, when the damping force is ideally nil. According to Ziyaeifar and Noguchi [3], in partial mass isolation, a high damping force reduces the isolation effect, blocking the sliding gap offered by the isolation layer. This fact practically sets a limit for the appropriate value of the linear damping ratio, which may be increased when a non-linear viscous device is used, as it is capable of providing lower damping force together with a higher energy dissipation rate. However, tests conducted by Wolff et al. [21], who compared the effectiveness of linear and non-linear FVDs, used together with low damping rubber bearings and high damping FPS isolators, showed that linear damping is more suitable to contain increases in inter-storey drift and floor acceleration, particularly in the case of high damping isolators, despite the apparent advantages of non-linear devices.

Although not new, this topic is still of great interest. The main effects of additional damping on base-isolated buildings are clear, but recent results obtained by several authors are not always easy to compare, because they are also strongly influenced by the initial hypotheses, including damper features. In addition, the use of FVDs in buildings isolated at storey level, rather than at the base, has its own peculiarities, and the effectiveness of FVDs for the improved seismic performance of such structures has not yet been investigated.

Within this context, this paper presents a multi-objective optimization study of an FVD mounted on an inter-storey isolation system, consisting of both natural rubber bearings (NRBs) and lead rubber bearings (LRBs). For this purpose, a reference seven-storey building was examined, with substructure and superstructure modelled as linear and separated between the second and third floors by an isolation layer with non-linear hysteretic behaviour depending on both displacement (due to LRBs) and velocity (due to the FVD). Time-history simulations were performed for various natural accelerograms, scaled to the same peak ground acceleration (PGA) of 0.25 g, for comparison. Although several multi-objective structural optimization studies have been carried out over the last 20 years, this type of investigation, to the authors' knowledge, still seems to be missing in the scientific literature. For example, as regards storey isolation, optimization studies concern the number and position of the isolation layers along the height of the building [24,25] and the properties of its isolators [8,26]; whereas, as regards FVDs, these studies concern their optimal allocation inside buildings [27] and optimal parameters in controlling vibration in stay cables for bridges [28,29], but only a few of them deal with FVD optimization when used together with isolators, and they also focus only on linear dampers [30]. Indeed, previous studies of the effectiveness of additional damping in base-isolated buildings have always been addressed by assuming FVD features. In particular, in this study, the fast, elitist Non-dominated Sorting Genetic Algorithm NSGA-II [31] was used to find a set of optimal Pareto solutions, or optimal combinations of damper parameters, i.e., damping coefficient c (ranging from 1 to 10^7 N(s/m) ^{α}) and exponent α (0.1–1.0). For this purpose, two objective functions were chosen and pursued simultaneously, which are: minimisation of isolation layer deflection, and minimisation of total superstructure drift. Furthermore, the following constraint was assumed in the analysis: the total drift of the superstructure must be limited to that calculated without using FVDs. The results show the potential of optimal FVDs in improving the seismic response of isolated inter-storey buildings, and include the maximum values of base shear force, FVD force, inter-storey drift and floor acceleration of both superstructure and substructure, shown as ratios between the cases with and without dampers, and plotted versus isolator drift reduction due to the dampers. Certain correlations between the frequency-domain velocity response of the isolation layer and the linearity degree and performance of the FVD are highlighted, and show that optimal α depends to a great extent on the non-linear seismic response of the structure, and thus on seismic action. Lastly, the design consequences of these research findings are discussed.

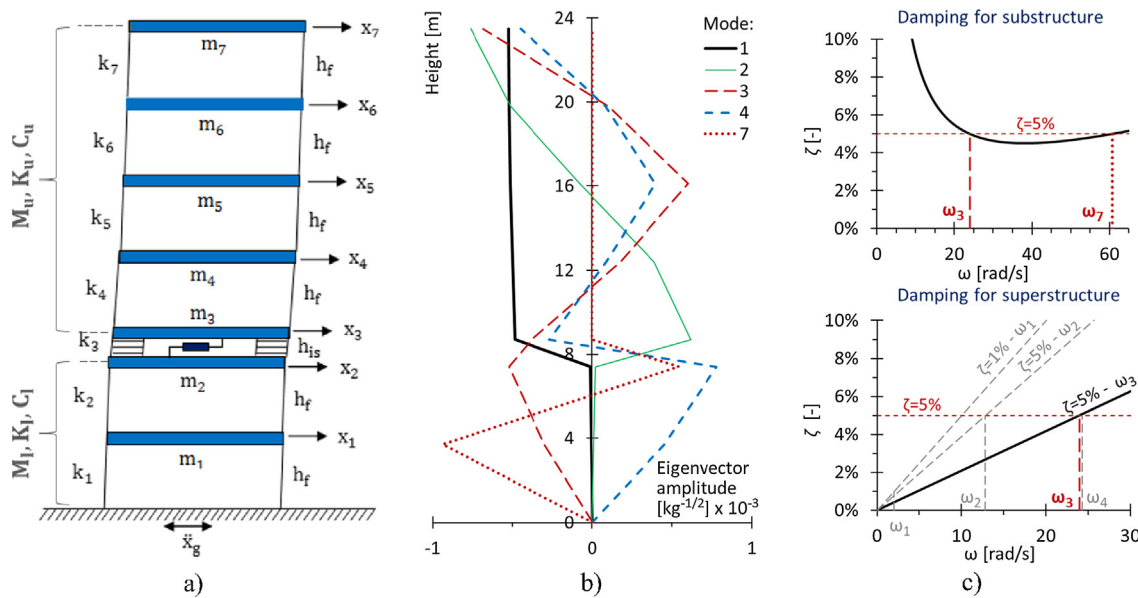


Fig. 1. (a) Seven-storey building model with storey isolation; (b) modal shapes considering LRBs yielded; (c) damping models assumed for substructure (Rayleigh) and superstructure (proportional to stiffness).

2. Case study: building model and seismic input

2.1. Storey-isolated building model

The building model examined here is shown in Fig. 1(a). It includes a two-floor substructure and a five-floor superstructure elevated above the storey-isolation system.

The isolated superstructure (including the isolation system) is very similar to an existing base-isolated office building with an RC frame structure, whereas the substructure is ideal and was chosen for the purposes of this study, considering a different structural solution with respect to the superstructure. That is, the masses of the first and second floors are similar to those of the upper storeys, whereas the storey lateral stiffness of the substructure is about three times higher than that of the first superstructure storey, as shown in Table 1: this shows the case of a lightweight substructure used for commercial purposes, with a floor extension larger than that of the RC superstructure. This type of irregular building in elevation, with an office or residential multi-storey RC building constructed over a wider substructure of different use and material, is increasingly common in highly populated residential areas (as is the case in China). In addition, growing interest and greater confidence in the storey-isolation technique are becoming evident.

The isolation system, consisting of LRBs and NRBs, which are the most commonly used isolators in China, is considered to be placed between the second and third slabs. A total number of 14 LRBs and 6 NRBs were installed in the real project, providing an overall elastic stiffness k of the isolation system of 118.4 kN/mm and a post-yield stiffness rk of 16.7 kN/mm (i.e., a post-yielding stiffness ratio r of 0.141). These values are assumed for the isolation system of our case study, whose overall hysteretic characteristics are described below. The post-yield stiffness is such as to lead to a vibration period of the base-isolated structure of about 3 s.

Table 1
Stiffness, masses and height of building model.

| Storey (inter-storey height: $h_f = 3.7$ m, $h_{is} = 1.3$ m) | 1st | 2nd | 3rd | 4th | 5th | 6th | 7th |
|---|------|------|-----|-----|-----|-----|-----|
| Stiffness (kN/mm) | 1330 | 1140 | – | 380 | 300 | 300 | 250 |
| Mass (tons) | 850 | 850 | 960 | 830 | 800 | 800 | 500 |

A generic FVD is then added to the isolation layer, the parameters of which are calculated in the next section, to obtain optimal design solutions.

Table 2 (left) and Fig. 1(b) provide the main modal results, modal frequencies and shapes, respectively, considering post-yield stiffness rk of the isolation system; Table 2 also shows the modal contributions. The first mode is less representative of the overall dynamics of the building when compared with that of a base-isolated structural system equivalent to the superstructure. In addition, the most significant higher modes are the third and fourth, which have similar frequencies but different shapes: the fourth deforms the isolation layer to a greater extent.

The dynamic equation governing the motion of such a building model for each time instant t is:

$$\mathbf{M}\ddot{\mathbf{x}}(t) + \mathbf{C}_{st}\dot{\mathbf{x}}(t) + \mathbf{K}_{st}\mathbf{x}(t) + \mathbf{r}_{is}F_{is}(t) + \mathbf{r}_{vd}F_{vd}(t) = -\mathbf{M}\ddot{\mathbf{u}}_g(t) \quad (1)$$

$\mathbf{x}(t)$, $\dot{\mathbf{x}}(t)$, $\ddot{\mathbf{x}}(t)$, expressed as $[x_1(t) \ x_2(t) \ \dots \ x_7(t)]^T$ and so on, are the vectors of the relative storey displacement, velocity and acceleration, with respect to the base of the building and represent the output of the dynamic equation. $\ddot{\mathbf{u}}_g(t)$ is the acceleration time series of ground motion, and \mathbf{I} represents the unitary rigid displacement vector of the structure in the direction of the earthquake (horizontal) which, in this case study, is equal to the identity vector.

\mathbf{M} is the matrix of mass (of size $[7 \times 7]$), which can be directly

Table 2
Results of modal analysis (LRBs yielded) and structural damping ratios ζ_i (Eq. (6)) without LRBs and FVD.

| Mode | Angular frequency ω [rad/s] | Modal contribution [%] | $\zeta_{L,i}$ due to substructure [%] | $\zeta_{u,i}$ due to superstructure [%] | $\zeta_{Tot,i}$ due to total structure (without LRBs and FVD) [%] |
|------|------------------------------------|------------------------|---------------------------------------|---|---|
| 1 | 2.0 | 70.6 | 0.01 | 0.02 | 0.03 |
| 2 | 12.8 | 0.1 | 0.01 | 2.59 | 2.59 |
| 3 | 24.0 | 8.6 | 1.55 | 3.49 | 5.03 |
| 4 | 24.3 | 18.5 | 3.40 | 1.54 | 4.94 |
| 5 | 32.2 | 0.0 | 0.00 | 6.75 | 6.75 |
| 6 | 37.2 | 0.0 | 0.00 | 7.80 | 7.80 |
| 7 | 60.7 | 2.1 | 5.00 | 0.00 | 5.00 |

derived from Table 1. \mathbf{C}_{st} and \mathbf{K}_{st} are the matrixes of damping and stiffness of the building, without considering the isolation layer, and thus have the form:

$$\mathbf{K}_{st} = \begin{bmatrix} \mathbf{K}_l[2 \times 2] & \\ & \mathbf{K}_u[5 \times 5] \end{bmatrix}$$

$$\mathbf{C}_{st} = \begin{bmatrix} \mathbf{C}_l[2 \times 2] & \\ & \mathbf{C}_u[5 \times 5] \end{bmatrix} \quad (2)$$

where, \mathbf{K}_l and \mathbf{C}_l are the stiffness and damping matrixes for the lower (l) part of the building and \mathbf{K}_u and \mathbf{C}_u are the same matrixes for the upper (u) part.

\mathbf{K}_l and \mathbf{K}_u are directly obtained from the stiffness values of Table 1, as shown in Eq. (3).

$$\mathbf{K}_l = \begin{bmatrix} k_1 + k_2 & -k_2 \\ -k_2 & k_2 \end{bmatrix}$$

$$\mathbf{K}_u = \begin{bmatrix} k_4 & -k_4 & & & \\ -k_4 & k_4 + k_5 & -k_5 & & \\ & -k_5 & k_5 + k_6 & -k_6 & \\ & & -k_6 & k_6 + k_7 & -k_7 \\ & & & -k_7 & k_7 \end{bmatrix} \quad (3)$$

Equivalent viscous damping was modelled differently for the two structural parts (non-classical damping). In particular, the classic Rayleigh formulation (Eq. (4)) was assumed for the substructure, as is generally the case with fixed-base structures; instead, for the isolated superstructure, a more appropriate stiffness-proportional damping model (Eq. (5)) was adopted, according to Ryan and Polanco [32] and Pant et al. [33]. $\mathbf{M}_l [2 \times 2]$ and $\mathbf{M}_u [5 \times 5]$ are clearly the matrixes of mass for the two separated parts of the building. Rayleigh coefficients α_l and β_l were calibrated, as shown in Fig. 1(c), by associating a damping ratio ζ of 5% to the third and seventh mode frequencies (see Table 2), which define the significant vibrational range of the substructure. As regards the calibration of proportionality coefficient β_u , Pant et al. [33] suggested using $\zeta = 1\%$ at the first mode frequency (ω_1), obtained with the post-elastic stiffness of the isolation system, but also concluded that stiffness-proportional damping may suppress higher mode effects for tall base-isolated buildings, in which higher modes may be involved to a greater extent. The latter consideration thus becomes relevant in the case of storey isolation, due to the greater importance of higher modes. According to these considerations and the modal contributions shown in Table 2, it was decided to calibrate β_u considering $\zeta = 5\%$ at ω_3 , resulting in lower damping when compared with that suggested by Pant et al. [33] (which corresponds approximately to $\zeta = 5\%$ at ω_2 , as shown in Fig. 1(c)). To verify the goodness of these choices, Table 2 (right) lists modal damping ratios ζ_i due to the substructure [\mathbf{C}_l], superstructure [\mathbf{C}_u] and global structure [\mathbf{C}_{st}] alone (without isolation system), calculated according to the well-known Eq. (6) for classical damping (where ϕ_i and ω_i are the mode shape and angular frequency of mode i , respectively), thus neglecting the off-diagonal coupling terms (negligible) of the damping matrix expressed in modal coordinates. As can be seen, the value of ζ_i for the significant higher modes is about 5% (the usual value for RC structures), whereas that of the first mode turns out to be very small: this is correct, in view of the negligible contribution of deformation and thus damping, provided by the substructure and superstructure for this mode, compared with that of the isolation layer.

$$\mathbf{C}_l = \alpha_l \mathbf{M}_l + \beta_l \mathbf{K}_l$$

$$\rightarrow \alpha_l = 0.05 \cdot \frac{2\omega_3\omega_7}{\omega_3 + \omega_7}; \beta_l = 0.05 \cdot \frac{2}{\omega_3 + \omega_7} \quad (4)$$

$$\mathbf{C}_u = \beta_u \mathbf{K}_u \rightarrow \beta_u = 0.05 \cdot \frac{2}{\omega_3} \quad (5)$$

$$\zeta_i = \frac{\phi_i^T \mathbf{C}_i \phi_i}{2\omega_i \phi_i^T \mathbf{M}_i \phi_i} \quad (6)$$

Table 3
Values of Bouc-Wen model parameters.

| r [-] | k [kN/mm] | d_y [mm] | A [-] | β [-] | γ [-] | η [-] |
|------------|----------------|---------------|------------|----------------|-----------------|---------------|
| 0.141 | 118.4 | 7.8 | 1 | 1 | 1 | 2 |

The contribution of the isolation layer is described by the last two addenda of Eq. (1). In particular, force $F_{is}(t)$ developed by the isolation system, thus its dissipation, is modelled with the Bouc-Wen model [34]:

$$F_{is}(t) = r k x(t) + (1-r) k d_y z(t) \quad (7)$$

where r and k are respectively the post-yielding stiffness ratio and the elastic stiffness of the isolation system (specified above), and d_y is the yielding displacement of the LRBs, which is 7.8 mm in this case study. Instead, $z(t)$ is a function of time defining hysteretic behaviour, and must satisfy the following non-linear first-order differential equation:

$$\dot{z}(t) = \frac{1}{d_y} (A \dot{x}(t) - \beta |\dot{x}(t)| z(t) |z(t)|^{\eta-1} - \gamma \dot{x}(t) |z(t)|^\eta) \quad (8)$$

A , β , γ and η are non-dimensional parameters influencing the hysteretic loop shape [35]. Their values, shown in Table 3 together with the other Bouc-Wen model parameters, were chosen to simulate the experimental force-displacement loops provided by Kalpakidis and Constantinou [36, p.132], resulting from a sinusoidal test (frequency 0.35 Hz, amplitude 114 mm, LRB-diameter 500 mm) fairly representative of our case study.

Lastly, the damping force $F_{vd}(t)$ developed by the FVD is calculated as:

$$F_{vd}(t) = c |\dot{x}|^\alpha \text{sgn}(\dot{x}) \quad (9)$$

where, c and α are the damping coefficient and exponent, respectively.

To correctly consider the contributions of isolators and damper, in terms of position in the motion equation, influence vectors \mathbf{r}_{is} and \mathbf{r}_{vd} , which are equal in this study, are introduced:

$$\mathbf{r}_{is} = \mathbf{r}_{vd} = [0 \quad -1 \quad 1 \quad 0 \quad 0 \quad 0 \quad 0]^T \quad (10)$$

The total restoring force $F_r(t)$ provided by the structure, according to Eq. (11), can be subdivided into two contributions: one linear, due to the elastic stiffness of both building and isolators \mathbf{K} , and one non-linear, provided only by the hysteretic behaviour of the isolators (see Eq. (7)):

$$\mathbf{F}_r(t) = \mathbf{K}_{st} \mathbf{x}(t) + \mathbf{r}_{is} F_{is}(t) = \mathbf{K} \mathbf{x}(t) + \mathbf{r}_{is} (1-r) k d_y z(t) \quad (11)$$

$$\mathbf{K} = \begin{bmatrix} k_1 + k_2 & -k_2 & 0 & \dots & 0 \\ -k_2 & k_2 + r k & -r k & & \vdots \\ 0 & -r k & r k + k_4 & -k_4 & \\ \vdots & & & \ddots & 0 \\ & & -k_6 & k_6 + k_7 & -k_7 \\ 0 & \dots & 0 & -k_7 & k_7 \end{bmatrix} \quad (12)$$

Substituting Eq. (11) in Eq. (1), we can write:

$$\mathbf{M} \ddot{\mathbf{x}}(t) + \mathbf{C}_{st} \dot{\mathbf{x}}(t) + \mathbf{K} \mathbf{x}(t) + \mathbf{r}_{is} (1-r) k d_y z(t) + \mathbf{r}_{vd} F_{vd}(t) = -\mathbf{M} \ddot{u}_g(t) \quad (13)$$

from which, solving for $\ddot{\mathbf{x}}(t)$, we obtain:

$$\ddot{\mathbf{x}}(t) = -\mathbf{M}^{-1} (\mathbf{C}_{st} \dot{\mathbf{x}}(t) + \mathbf{K} \mathbf{x}(t) + \mathbf{r}_{is} (1-r) k d_y z(t) + \mathbf{r}_{vd} F_{vd}(t)) - \ddot{u}_g(t) \quad (14)$$

Lastly, introducing the state space vector $\mathbf{q}(t) = [\mathbf{x}^T(t) \dot{\mathbf{x}}^T(t) z(t)]^T$, Eq. (1) can be more conveniently expressed as a first-order differential equation in state space, as below:

$$\dot{\mathbf{q}}(t) = [\dot{\mathbf{x}}^T(t) \ddot{\mathbf{x}}^T(t) \dot{z}(t)]^T = \mathbf{f}(\mathbf{q}(t)) - \mathbf{B} \ddot{u}_g(t) \quad (15)$$

where $\mathbf{f}(\mathbf{q}(t))$ is a vector expressed as a function of state space vector $\mathbf{q}(t)$ and \mathbf{B} is a vector needed to take into account the correct position of

Table 4
Main details of natural earthquakes examined (from PEER database [37]).

| Earthquake | Location | Date | Mw | Distance from epicentre [km] |
|-----------------------|------------|------------|-----|------------------------------|
| 1. Big Bear | California | 1992/06/28 | 6.5 | 45 |
| 2. Superstition Hills | California | 1987/11/24 | 6.2 | 18 |
| 3. Duzce | Turkey | 1999/11/12 | 7.1 | 26 |
| 4. North Palm Springs | California | 1986/07/08 | 6.1 | 42 |
| 5. San Fernando | California | 1971/02/09 | 6.6 | 23 |
| 6. Chi-Chi | Taiwan | 1999/09/20 | 6.3 | 84 |
| 7. Imperial Valley | California | 1979/10/15 | 6.5 | 22 |
| 8. Irpinia | Italy | 1980/11/23 | 6.9 | 10 |

ground acceleration in the equation.

$$\mathbf{f}(\mathbf{q}(t)) = \begin{bmatrix} \dot{\mathbf{x}}^T(t) \\ -\mathbf{M}^{-1}(\mathbf{C}_{st}\dot{\mathbf{x}}(t) + \mathbf{K}\mathbf{x}(t) + \mathbf{r}_{is}(1-r)kd_y z(t) + \mathbf{r}_{vd}\mathbf{F}_{vd}(t)) \\ \frac{1}{d_y}(A\dot{\mathbf{x}}(t) - \beta |\dot{\mathbf{x}}(t)| z(t)|z(t)|^{p-1} - \gamma\dot{\mathbf{x}}(t)|z(t)|^p) \end{bmatrix} \quad (16)$$

$$\mathbf{B} = [\mathbf{0} \quad \mathbf{I} \quad \mathbf{0}]^T \quad (17)$$

2.2. Natural records examined

Eight different seismic inputs, chosen between the available natural records of the PEER database [37], were implemented in Eq. (15) to solve the dynamic equation of motion (or time-history analysis). Their main details are shown in Table 4.

For purposes of comparison, all these natural records were scaled to the same PGA of 0.25 g. Fig. 2 shows the acceleration and displacement spectra of these scaled earthquakes.

3. Multi-objective optimal design of additional FVDs

3.1. Objective functions and NSGA-II genetic algorithm

The following calculations aimed at obtaining optimal design solutions for the additional FVD; in other words, at finding the optimal combinations of the FVD parameters, i.e., damping coefficient *c* and exponent *α*. For this purpose, some design aims had to be defined, generally related to minimisation of structural response parameters.

For example, studying the most effective position of isolation layers throughout the height of a given building, Charmpis et al. [24] proposed an elaborate objective function to minimise maximum floor accelerations, with constraints on the maximum inter-storey drift, base displacement and the cost of isolators. Reggio and De Angelis [8] and

Zhou et al. [26], who proposed analytical approaches to calculate the optimal parameters of a mid-storey isolation system (using a simpler reduced-order two-DOF model), considered as their design aim the maximization of an energy performance index and the minimisation of the maximum base shear force, respectively.

The main function of an FVD mounted in an inter-storey isolation system is reduction of isolator deflection to minimise P-Δ effects on the substructure; however, as shown in the scientific literature, extra damping may be detrimental, because it may increase inter-storey drifts and internal forces of the isolated structure. The optimal design presented here aimed at combining the following two objective functions (OFs) simultaneously:

- minimisation of the relative displacement of isolation layer *OF₁*;
- minimisation of the total drift of superstructure *OF₂*.

A constrain condition, limiting the maximum total drift of superstructure *OF_{2,max}* to the maximum value reached in the case of isolation without FVD, was also assumed. The *OFs* and the constraint are shown in Eqs. (18) and (19):

$$OF_1 = \min |d_{iso}^D| = \min |x_3(t) - x_2(t)| \quad (18)$$

$$OF_2 = \min |d_{sup}^D| = \min |x_7(t) - x_3(t)|; OF_{2,max} \leq d_{sup} \quad (19)$$

where *d_{iso}^D* and *d_{sup}^D* represent the total drift of the isolators and superstructure in the case of isolation system with FVD, respectively; *d_{iso}* (used later in Figs. 5 and 6) and *d_{sup}* represent the same parameters for the case without FVD.

Although maximum storey acceleration is an important parameter of structural performance, particularly for seismic protection of structural contents, it was not within the optimization criteria, but only verified as an output of the optimization problem, in order to obtain a wider range of technically optimal solutions, for more comprehensive assessment of the potential of the extra FVD. In addition, technical

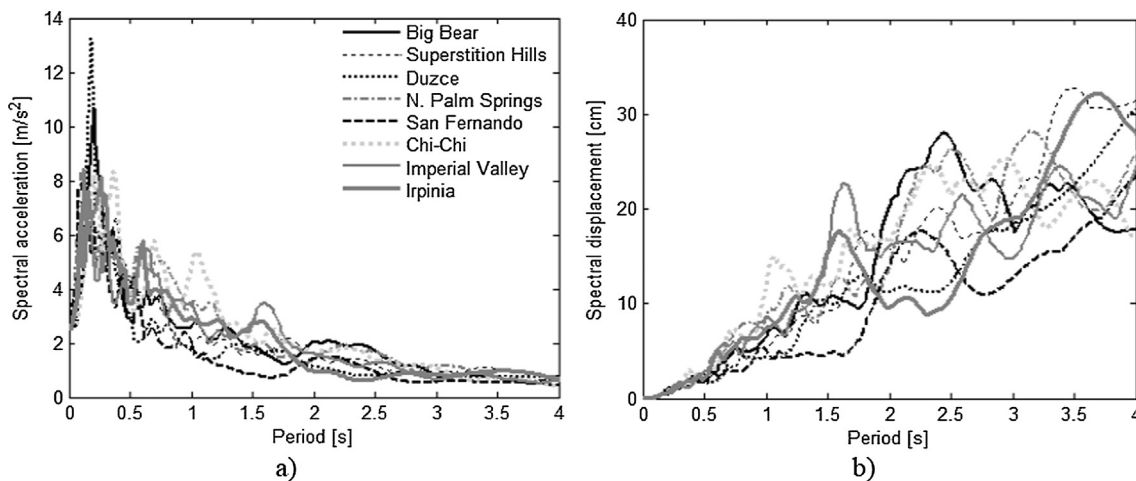


Fig. 2. Acceleration and displacement spectra of scaled natural records.

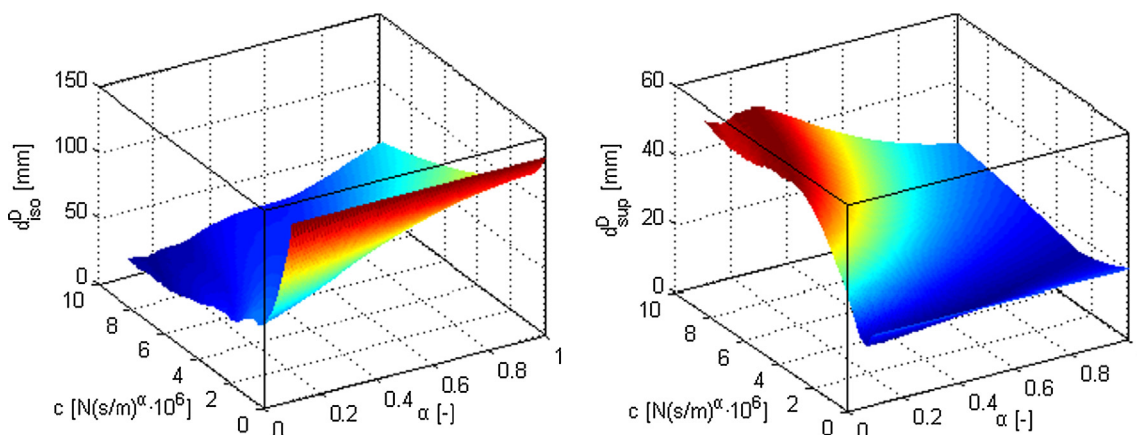


Fig. 3. Conflicting aspects of two objective functions OF_1 and OF_2 of Eqs. (18) and (19), for Superstition Hills earthquake.

effectiveness is not the only discriminating factor in choosing the best design solution, as technical feasibility (e.g., maximum deformation of isolation units) and costs must also be considered. Therefore, since these aspects may also easily be verified subsequently for the technically optimal solutions obtained, a wider range of possible optimal solutions is preferable, compared with a few solutions which optimize many objective functions. Although this paper mainly focuses on aspects of technical effectiveness, the main design consequences of the results shown below are discussed in Section 6.

The optimal values of the damper parameters were sought within the following ranges: from 0.1 to 1.0 for α and from 1.0 to 10^7 Ns/m for c . The conflicting aspects of the two objective functions are shown in Fig. 3, in which the solutions to Eq. (15) appear in terms of d_{iso}^D and d_{sup}^D for the Superstition Hills earthquake and for all assumed ranges of c and α .

The presence of multiple goals in solving a generic problem means that a set of optimal solutions (also known as Pareto-optimal solutions) must be obtained, instead of just one optimal solution. In general, if no additional information is specified, none of these optimal solutions can be considered better than another one, and this therefore requires the determination of all possible Pareto-optimal solutions. Many multi-objective evolutionary algorithms are now available [38] and these multiple solutions can be found in a single simulation run.

Among these algorithms, the fast and elitist Non-dominated Sorting Genetic Algorithm NSGA-II [31] has been widely used in practical optimization problems, and it was also chosen for the present study. First, this algorithm creates an initial random parent population P_0 , of size N . This population is then sorted according to the non-domination criterion, assigning to each solution a rank (fitness) equal to its non-domination level (1 is the best level, 2 the next-best, and so on) and minimising it. An offspring population Q_0 , of size N , is then created by binary tournament selection, recombination and mutation operators. The generation at step $k + 1$, starting from knowledge of the parent (P) and offspring (Q) populations at step k , is summarised below:

- a combined population R_k of size $2N$, resulting from the combination of P_k and Q_k , is formed;
- the solutions of the new population P_{k+1} , of size N , are chosen from those of R_k based on two cascading criteria: of the solutions with different non-domination rank, the one with lower (better) rank is chosen; between solutions with the same rank, the one located in a less crowded region is preferred, chosen by a crowded-comparison operator;
- the new population P_{k+1} is now used for binary tournament selection, crossover and mutation, to create a new offspring population Q_{k+1} of size N ; in this step, the crowded-comparison operator is still used in the selection procedure, thus preserving diversity among non-dominated solutions.

This procedure is continued for a certain number of generations until the Pareto front becomes stable, yielding the required optimal solutions. In this study, the number of generations and the population size were set at 100 and 80, respectively. Table 5 also shows the other main parameters assumed for the optimization algorithm.

To examine the constraint of Eq. (19), i.e., that d_{sup}^D must be smaller than d_{sup} , the simple penalty function approach of Eq. (20) was used, in which a penalty factor P (of a sufficiently large value) is added to parameters d_{iso}^D and d_{sup}^D of the candidate solutions (c, α) which do not meet this condition, in order to discard them from the generation of the next population.

$$\text{if } d_{sup}^D > d_{sup} \begin{cases} d_{iso, new}^D = d_{iso}^D + P \\ d_{sup, new}^D = d_{sup}^D + P \end{cases} \quad (20)$$

Time-history dynamic analyses (THAs) of the storey-isolated building are performed by MATLAB software, solving Eq. (15) by a custom-made code. This code is iteratively called by the optimization algorithm, which is also implemented in a MATLAB code, in order to find the Pareto-optimal solutions. For candidate solutions, the optimization code prepares the set of damper parameters to be inserted in the dynamic analysis program, which then computes the corresponding time-history responses. The THA results, expressed in terms of OFs, are sent to the optimization code to determine the new candidate optimal solutions.

3.2. Optimal designs and parameters of additional FVD

An example of the optimization algorithm iterations is shown in Fig. 4 for the Superstition Hills earthquake. The initial generation (Fig. 4(a)) shows some high values for OF_1 and OF_2 , because of the penalty function applied to candidate solutions exceeding the limit of superstructure drift. However, these values fall very quickly and, immediately after the first iterations, all candidate optimal solutions meet the imposed constraint (Fig. 4(b)). In addition, the improvement in the solutions is faster for the first generations than for the later ones, in which the populations are closer to the Pareto optimal front, as Fig. 4(c) and (d) shows.

Fig. 5 shows the Pareto fronts obtained for all analysed earthquakes.

Table 5
Parameters for optimization algorithm NSGA-II [31].

| Parameter | Value |
|-----------------------|-------|
| Number of generations | 100 |
| Population size | 80 |
| Crossover probability | 0.9 |
| Mutation probability | 0.1 |

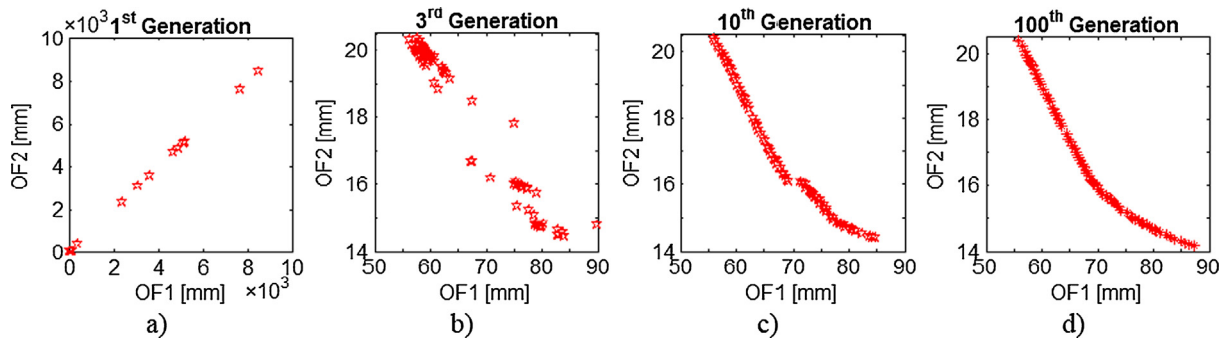


Fig. 4. Evolution of Pareto-optimal solutions for Superstition Hills earthquake.

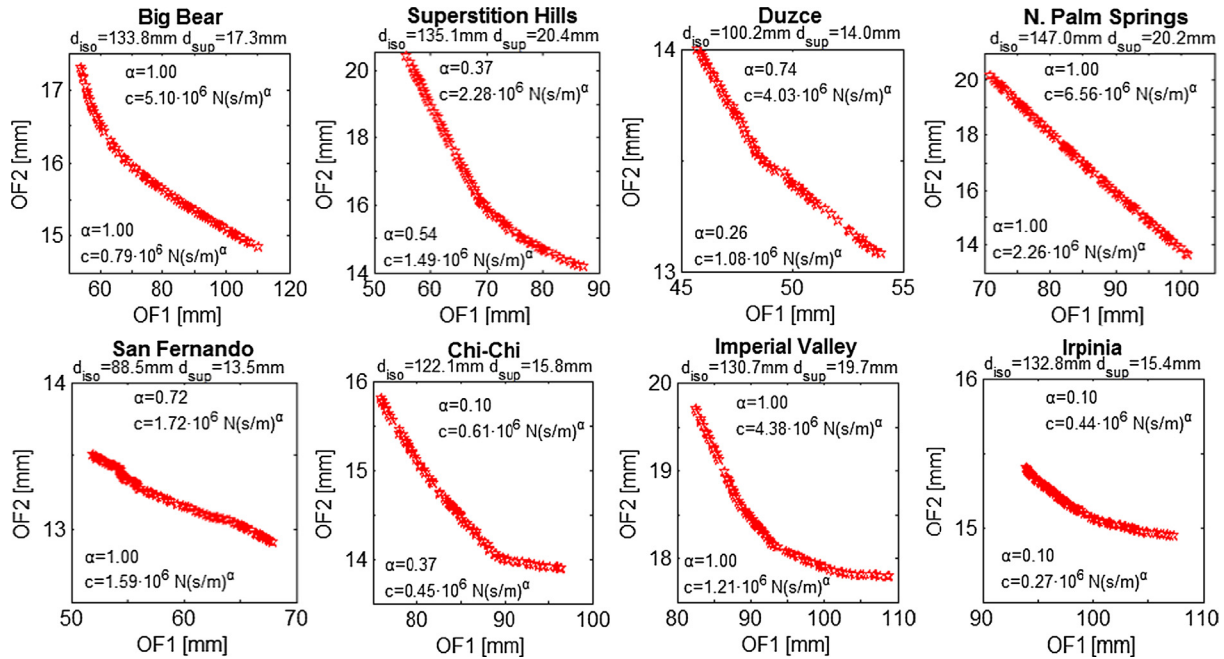


Fig. 5. Pareto front for earthquakes analysed, with indication of: d_{iso} and d_{sup} , i.e., isolators and superstructure drift in the case without FVD; c and α , related to cases of minimum OF_1 (top) and maximum OF_1 (below).

These optimal solutions are expressed in terms of the value of objective functions. The shape of these fronts is consistent with the conflicting aspects shown in Fig. 3, i.e., reduction in the relative displacement of isolation system OF_1 corresponds to an increase in superstructure drift OF_2 . For purposes of comparison, all the previous results are also plotted together in the dimensionless graph of Fig. 6, which presents ratio OF_2/d_{sup} versus ratio OF_1/d_{iso} , directly showing the reduction in drift due to the presence of the FVD, for both the isolation layer and the superstructure and for all earthquakes. As shown in Fig. 6, in some cases supplemental damping can greatly reduce isolator displacement (OF_1), while ensuring, at most, the same total drift of the superstructure, with a reduction of up to 60%, as in the cases of the Big Bear and Superstition Hills earthquakes. However, at other times, this reduction is much lower, indicating that extra damping may sometimes be effective only at the expense of an increase in superstructure drift.

Fig. 7 shows the FVD parameters (damping exponent α and damping coefficient c) required to obtain these Pareto-optimal solutions, i.e., the output of the multi-objective design. The figure clearly shows that the best performance of additional damping can be reached either by linear ($\alpha \approx 1$) or non-linear ($\alpha < 1$) viscous dampers, depending on the type of earthquake.

Because optimal FVD performance and parameters depend to a great extent on the type of earthquake, Section 5 expands these relationships in some interesting correlations.

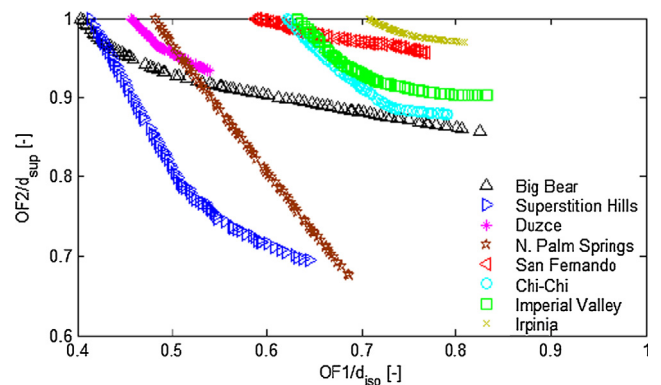


Fig. 6. Optimal solutions for OF_1 and OF_2 , normalised to related drifts d_{iso} , d_{sup} obtained without FVD.

4. Assessment of building behaviour with optimal FVDs

4.1. Building behaviour minimising isolator drift

The results presented in this section demonstrate building behaviour when the optimal FVD used is the one that minimises the relative displacement of the isolation system; in other words, for the optimal

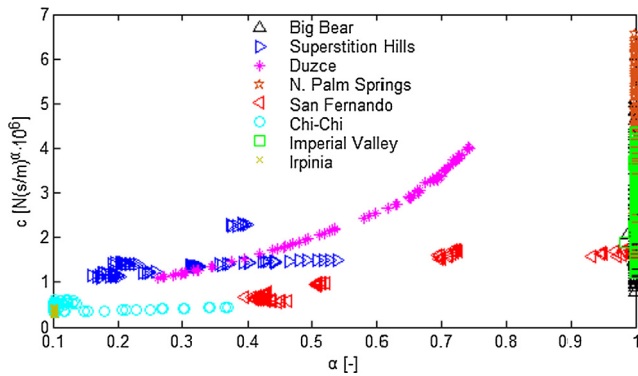


Fig. 7. Damping exponents α and coefficients c of FVD, associated with optimal solutions found.

solution with the minimum value of OF_I ($OF_{I,min}$) or $OF_2/d_{sup} = 1$.

In detail, Fig. 8 shows time-history responses in the case of the Big Bear earthquake, in terms of total drift of the superstructure and relative displacement of the isolators, comparing the case without and with FVD. As expected from previous results, extra damping greatly reduces isolator drift throughout the time interval of the earthquake, but slightly amplifies the total drift of the superstructure (particularly at the onset of the earthquake, in this case), although its maximum value is limited to that obtained in the case of isolation without FVD (due to the constraint set). The great reduction in isolator drift is also clear in Fig. 9, which compares force-drift loops of the isolation system for cases without and with FVD: in the latter case, the increase in damping ratio is evident, although the total force is slightly less.

The multi-objective design, considering drift minimisation of both isolators and superstructure, should lead to containment of shear forces at the base of the building. A first check on how this parameter is affected by additional damping is shown in Fig. 10, which shows the time-history response of this parameter for the Big Bear earthquake, and compares cases without and with FVD. The results confirm that, if the superstructure response is appropriately managed by FVDs inserted

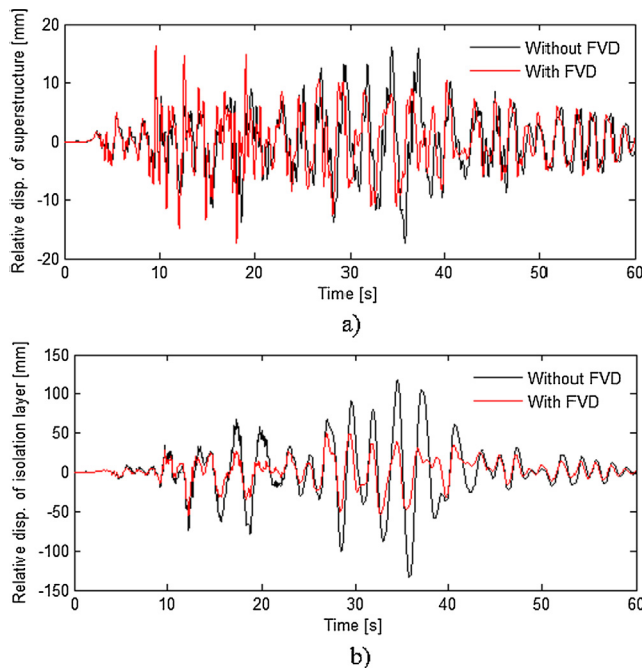


Fig. 8. Big Bear earthquake: (a) total drift of superstructure, and (b) relative displacement of isolators, with comparison between case without and with FVD (optimal solution for $OF_{I,min}$).

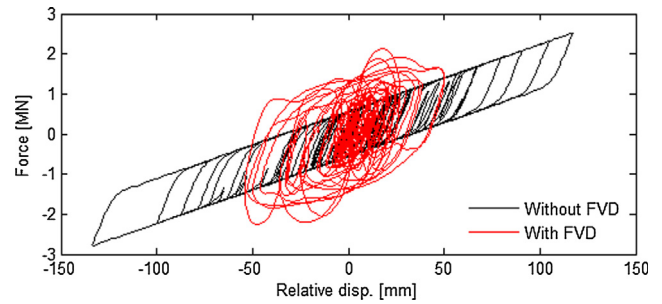


Fig. 9. Big Bear earthquake: force–displacement hysteretic loop of isolation system, for cases without and with FVD (optimal solution for $OF_{I,min}$).

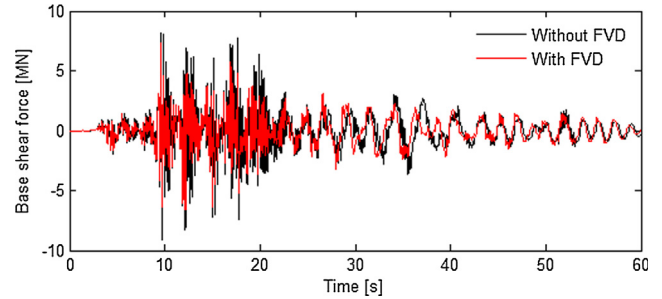


Fig. 10. Big Bear earthquake: shear force at base of building, for cases without and with FVD (optimal solution for $OF_{I,min}$).

in the isolation system, they can also effectively reduce shear forces at the base of the building.

Table 6 lists the results obtained for the extra damping effects on both isolator drift and base shear force for all earthquakes analysed, comparing the case without damper with that in which optimal FVD minimises OF_I .

Although only the total drift of the isolation layer and superstructure were examined as OFs in this multi-objective design, some other parameters also had to be checked, e.g., maximum floor acceleration and maximum inter-storey drift. In particular, to prevent critical damage to valuable building contents during an earthquake, a maximum allowable value for absolute floor accelerations is considered in practice, and this value is typically 0.2–0.3 g, according to contents [24]. For some highly vulnerable special contents, such as precious works of art or other unique objects, this value may be much lower. However, in this case, specific isolation techniques directly applied to the contents are available [39,40].

Figs. 11–14 show absolute peak and RMS (Root-Mean-Square average) storey accelerations, together with maximum inter-storey displacements and drift ratios, along the building height and for two representative earthquakes, comparing cases without and with FVD (for the latter, the optimal solution for $OF_{I,min}$ is still considered). The results confirm not only that supplementary damping may increase the maximum accelerations and drifts of the superstructure, but also that it is beneficial for the substructure, particularly when it is relatively high, as in the Big Bear case (see next section).

Although the increase obtained for these performance parameters of the superstructure seems moderate, even in absolute terms, sometimes it may be not acceptable, due to specific design requirements. Since these performance parameters are closely related to the added amount of supplementary damping, which has the effect of locking the sliding gap offered by the isolation layer [3], it would be interesting to evaluate their variability versus reduced damper performance in terms of minimisation of isolator drift (i.e., introducing less damping), considering all obtained optimal solutions, as presented below.

Table 6
Reduction of isolator drift and base shear force, with optimal solution for $OF_{I,min}$.

| Earthquake | α [-] | c [N/(s/m) ² ·10 ⁶] | Isolator drift [mm] | | | Base shear force [MN] | | |
|--------------------|--------------|--|---------------------|----------|-----------|-----------------------|----------|-----------|
| | | | No FVD | With FVD | Reduction | No FVD | With FVD | Reduction |
| Big Bear | 0.999 | 5.095 | 133.8 | 54.0 | -60% | 9.2 | 7.3 | -21% |
| Superstition Hills | 0.373 | 2.283 | 135.1 | 55.9 | -59% | 9.9 | 8.3 | -16% |
| Duzce | 0.742 | 4.028 | 100.2 | 45.7 | -54% | 9.3 | 7.8 | -16% |
| North Palm Springs | 0.999 | 6.560 | 147.0 | 70.9 | -52% | 6.5 | 5.8 | -11% |
| San Fernando | 0.718 | 1.717 | 88.5 | 52.0 | -41% | 6.8 | 5.8 | -15% |
| Chi-Chi | 0.100 | 0.606 | 122.1 | 75.9 | -38% | 9.0 | 8.6 | -5% |
| Imperial Valley | 1.000 | 4.380 | 130.7 | 82.5 | -37% | 5.1 | 5.2 | +2% |
| Irpinia | 0.100 | 0.435 | 132.8 | 93.9 | -29% | 11.0 | 9.6 | -13% |

4.2. Assessment of various optimal design solutions

As excessive damping leads to undesirable effects on the superstructure, in terms of maximum storey accelerations and inter-storey drifts, the most appropriate FVD may not be the one which minimises OF_I , which provides the greatest supplementary damping of all the optimal FVDs determined.

A comprehensive view of the trend of these performance parameters, for both substructure and superstructure, is therefore shown in Figs. 15 and 16. In particular, Fig. 15 shows the trend of the ratio between maximum floor accelerations, with and without FVD, versus the reduction in isolator drift; Fig. 16 shows the trend of a similar ratio, but examining maximum inter-storey drifts, with and without FVD. As regards the substructure, both these ratios generally have values lower than 1, together with less influence on damper performance when compared with those of the superstructure (particularly as regards the acceleration ratio). These trends indicate that, if a slightly smaller reduction in isolator drift is accepted, then the highest values of these ratios for the superstructure can effectively be reduced, if they are excessive or in the case of explicit design requirements, without significantly affecting the response of the substructure. Such a representation of the results can thus help in choosing the best solution among all the optimal ones obtained, taking into consideration design requirements on a case-by-case basis.

Fig. 17(a) shows the ratio between the maximum base shear forces, in cases with and without FVD, versus the drift reduction of the isolators. For each earthquake, the optimal solution with the maximum amount of additional damping ($OF_{I,min}$) is generally that with the lowest base shear force. In addition, for all the obtained optimal designs, except the Imperial Valley case, the maximum value of the base shear force is smaller when FVDs are used. Lastly, Fig. 17(b) shows the trend of the maximum FVD force, which increases more than linearly with decreasing isolator drift. These results are significant and may

affect the choice of the optimal damper, as they are closely related to the cost of fluid viscous devices.

5. Examination of FVD parameters and performance

With the aim of examining the factors affecting the degree of linearity and the performance of FVDs, the main modal frequencies of the overall structure and superstructure only are shown in Table 7. Due to variations in isolator stiffness during the seismic response, two modal analyses were performed on the total structure, considering both initial (k) and post-yield (rk) stiffness of the isolation system and thus estimating a frequency range for vibrational modes.

Also, the Fast Fourier Transform (FFT) of the relative velocity signal of the isolation layer ($\dot{x}_3(t) - \dot{x}_2(t)$) is shown in Fig. 18 (left), for various earthquakes and for cases without and with FVD (for optimal solution $OF_{I,min}$). The figure shows reductions in amplitude when dampers are used, in the vicinity of the main modal frequencies of the overall structure, which demonstrates the effectiveness of FVDs in mitigating the seismic response. In addition, the following interesting correlations with linearity degree α and the performance of the optimal FVDs can be observed.

- When the FFT signal in the damper case is examined, if the ideal envelope constructed on the velocity peaks shows a rapid monotonic increment up to maximum-peak frequency, followed by an equally rapid monotonic decrement for higher frequencies, optimal damping exponent α tends to be 1, i.e., the optimal damper tends to be linear. Vice versa, if the FFT signal presents equally important peaks in the frequency range of the first mode, i.e., its envelope has one or more plateaus, optimal α tends to be lower than 1, i.e., the optimal FVD is non-linear. Therefore, a linear FVD turns out to be preferable when the relative motion of the isolation layer tends to be dominated by one main frequency, so that the linearity of the

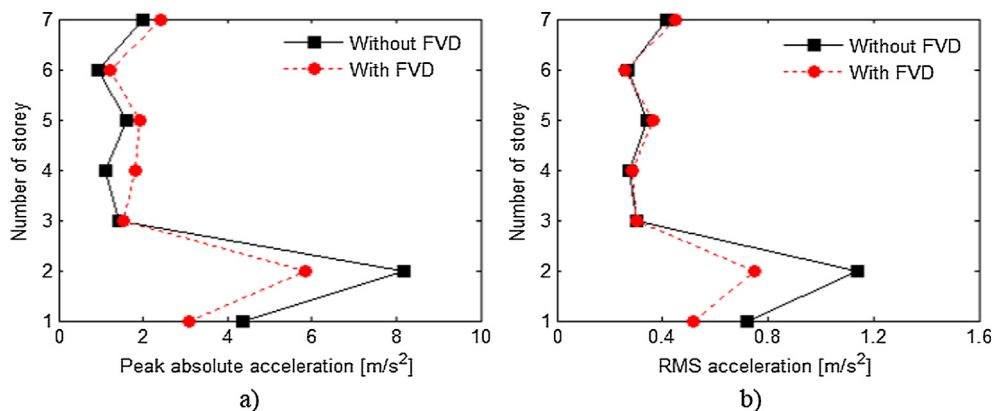


Fig. 11. Big Bear earthquake: (a) absolute peak acceleration, and (b) RMS acceleration along building height: comparison between case without and with FVD ($OF_{I,min}$).

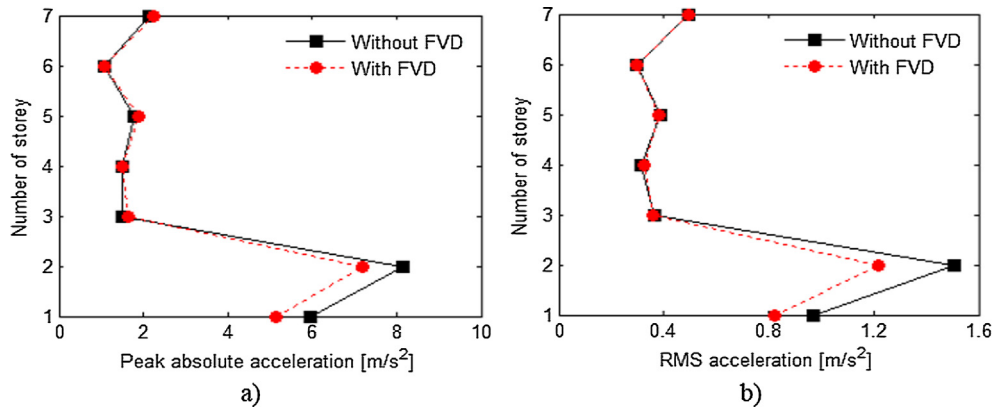


Fig. 12. Irpinia earthquake: (a) absolute peak acceleration, and (b) RMS acceleration along building height: comparison between case without and with FVD ($OF_{I,min}$).

damper can effectively contain force values at maximum displacements. As such a type of motion is generally representative for the base isolation case, this evidence seems to be consistent with the results of previous experimental studies on base-isolated structures [21] that prove the greater suitability of linear damping in containing increments of inter-storey drift and floor acceleration. In addition, these considerations lead to realise that optimal linearity degree of the extra FVD cannot easily be predicted in the case of inter-storey isolation, as it depends to a great extent on the non-linear seismic response of the structure with dampers. Fig. 18 (right) also shows separately the force-displacement (F-D) loops due to the isolation system and damper: the FVD loops associated with higher values of α are mainly characterized by almost concentric cycles, which increase in strength and displacement, whereas those related to lower values of α show a series of small cycles with barycenters which move along the displacement axis (e.g., compare Imperial Valley, $\alpha = 1.0$, and Irpinia, $\alpha = 0.1$, particularly at maximum displacement).

- An interesting correlation between the FFT signals and FVD performance, in terms of drift reduction of the isolators, can also be observed in the plots of Fig. 18, ranging from the best to the worst FVD performance: when the excited frequencies in the first-mode frequency range of the overall structure ($\sim 0.3\text{--}0.7$ Hz) increase, the performance of the FVD decreases, i.e., to comply with the constraint on the total drift of the superstructure, the allowed maximum reduction of isolator drift ($OF_{I,min}$) becomes smaller. This seems to be directly related to the maximum amount of supplementary damping which can be conveniently introduced into the isolation system, in view of its detrimental effects at higher modes [3,12,13,21]. In fact, when the main excited frequencies are lower

(i.e., the earthquake excites the isolators mainly during their behaviour with post-yield stiffness), the reduction in amplitude of the FFT signal due to the FVD is greater, indicating a greater amount of extra damping.

To prove the best performance of the FVD in the case of lower excited frequencies, two methods were applied to quantify the supplementary modal damping ratios for the analysed earthquakes, and the results are compared. One consists of applying complex modal analysis to estimate, for a certain mode i , damped angular frequency $\omega_{i,d}$, which, together with the corresponding undamped frequency $\omega_{i,u}$ obtained from classical eigenvalue analysis, allows us to estimate modal damping ratio ζ_i according to the following well-known formula:

$$\zeta_i = \sqrt{1 - \frac{\omega_{i,d}^2}{\omega_{i,u}^2}} \tag{21}$$

Complex modal analysis requires the definition of a damping matrix. To calculate damping ratios ζ_i due to structural damping only, matrix $[C_{st}]$ (as defined in Eq. (2)) can be used. Instead, to estimate the values of ζ_i provided by the overall structure, including the isolation layer, equivalent linear viscous damping coefficients c_{Eq} must be determined, for both isolators and FVD, and opportunely added to the previous matrix $[C_{st}]$ (i.e., $+c_{Eq}$, $-c_{Eq}$; $-c_{Eq}$, $+c_{Eq}$ in positions (2,2), (2,3); (3,2) (3,3)). The values of these coefficients (see Table 8) were determined in order to obtain the same maximum value of isolator drift when a linear viscous damping model is implemented in TH analysis, in place of the non-linear damping model initially adopted for the isolators or FVDs. In the case of linear optimal FVDs, c_{Eq} is directly the value of c of the damper. Once damping ratios are obtained for the cases with and without ($\zeta_{i,without}$) FVD, the additional damping contribution

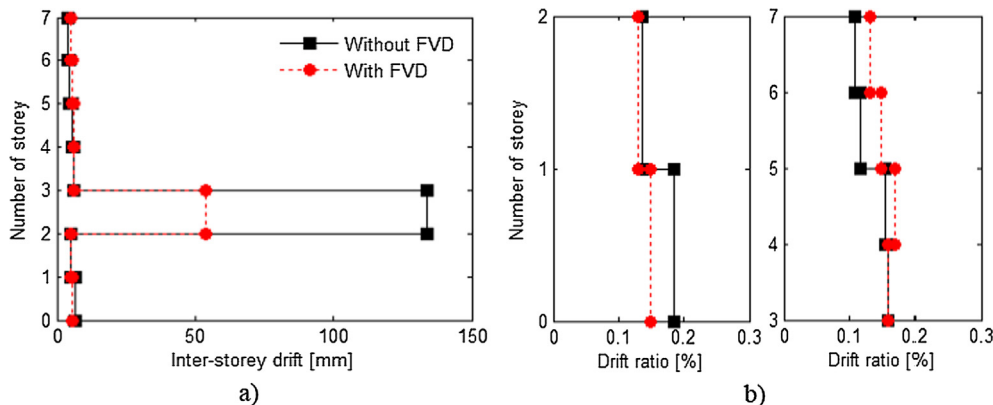


Fig. 13. Big Bear earthquake: (a) inter-storey displacement, and (b) drift ratio along building height: comparison between case without and with FVD ($OF_{I,min}$).

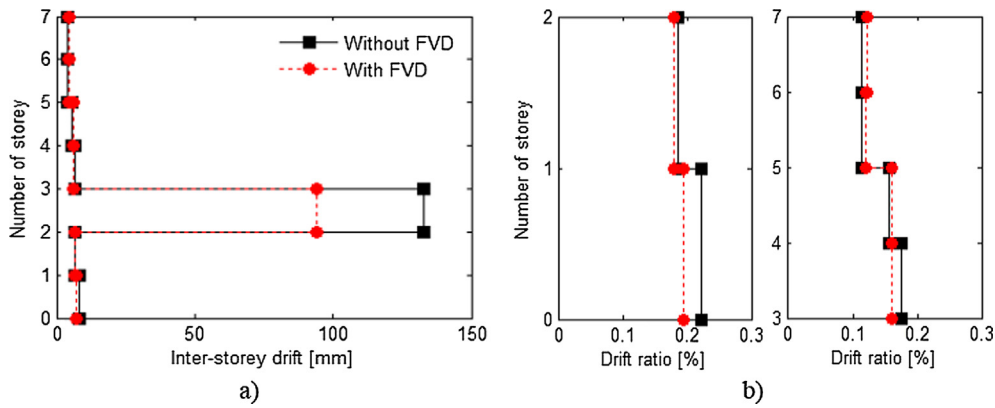


Fig. 14. Irpinia earthquake: (a) inter-storey displacement, and (b) drift ratio along building height: comparison between case without and with FVD ($OF_{1,min}$).

$\Delta\zeta_{1,FVD}$, due to the damper, can be calculated by the simple difference; these values, concerning only the first mode, i.e. $\zeta_{1,without}$ and $\Delta\zeta_{1,FVD}$, are listed in Table 9 (left).

Another method of estimating $\Delta\zeta_{1,FVD}$ is simply based on the damped response spectra of isolated superstructure, calculated from absolute accelerations of mass m_2 ($\ddot{x}_2(t) + \ddot{u}_g(t)$). Entering the damped spectra with the first mode displacement d_1 and period T_1 of the isolated superstructure, its first mode damping ratio ζ_1 , due to the isolation layer with and without FVD, can be estimated, as $\Delta\zeta_{1,FVD}$ by the difference. This method is quite simple but requires some attention in defining d_1 and T_1 . For typical base-isolated structures, without ‘too much damping’, d_1 can be estimated as the total displacement of the base, whereas with supplementary FVD, this simplification is no longer appropriate and second-mode effects must be taken into account in determining d_1 . As OF_1 corresponds to the total base displacement of the base-isolated superstructure, and the total superstructure drift OF_2 is due almost solely to the second mode, a sufficient approximation of d_1 would be $d_1 = OF_1 + OF_2/2$, since the second mode moves the top and base of the superstructure in the opposite direction by about the same amount ($OF_2/2$), reducing the base displacement due to the first mode (i.e., $d_1 - OF_2/2 = OF_1$). Regarding T_1 , its undamped or damped value may be used: although the latter is more appropriate, especially when supplementary damping is high (FVD- $OF_{1,min}$), the undamped period is easier to calculate and generally sufficient to obtain an acceptable estimate of ζ_1 . However, the damped period may be simply calculated iteratively, starting from the undamped period to estimate ζ_1 and then applying Eq. (21). An example of the application of this method is shown in Fig. 19 for the case of North Palm Springs.

The damping values resulting from the two methods, although not

equivalent, are correlated. ζ_1 evaluated by the spectral method is related to the dynamic response of the base-isolated superstructure, and thus to the total deformation of the isolation layer in the case of low damping (for which linear modal analysis is valid). Instead, ζ_1 obtained by complex modal analysis of the overall structure is related to only one part of this total deformation, corresponding to the first mode contribution factor (0.7; see Table 2) in the case of low damping. Therefore, if ζ_1 is calculated by the spectral method, it should be scaled by about 0.7 (contribution factor) to be expressed as an equivalent first-mode damping ratio of the overall structure, assuming for the sake of simplicity that this equivalence remains constant even in the case of high damping. The final values of $\zeta_{1,without}$ and $\Delta\zeta_{1,FVD}$ by the spectral method, i.e., scaled, obtained from undamped period T_1 , are also shown in Table 9 (right): these results are comparable with those from complex modal analysis.

According to the results shown in Table 9, the following considerations may be made.

- Damper performance, in terms of drift reduction of isolators in the case of $OF_{1,min}$, generally increases as supplementary damping increases: for the first four earthquakes in Table 9, with the best performance, $\Delta\zeta_{1,FVD}$ is generally greater than 30% (up to about 50%), whereas it is lower than 20% in the last four cases.
- The only exception is the Big Bear case, which showed the best FVD performance, although $\Delta\zeta_{1,FVD}$ was not very high (just under 30%). This is clearly related to the low damping provided by the isolation system ($\zeta_{1,without}$) which, for this earthquake, was the lowest of all cases.
- The damping ratio provided by the isolators ($\zeta_{1,without}$) ranges from

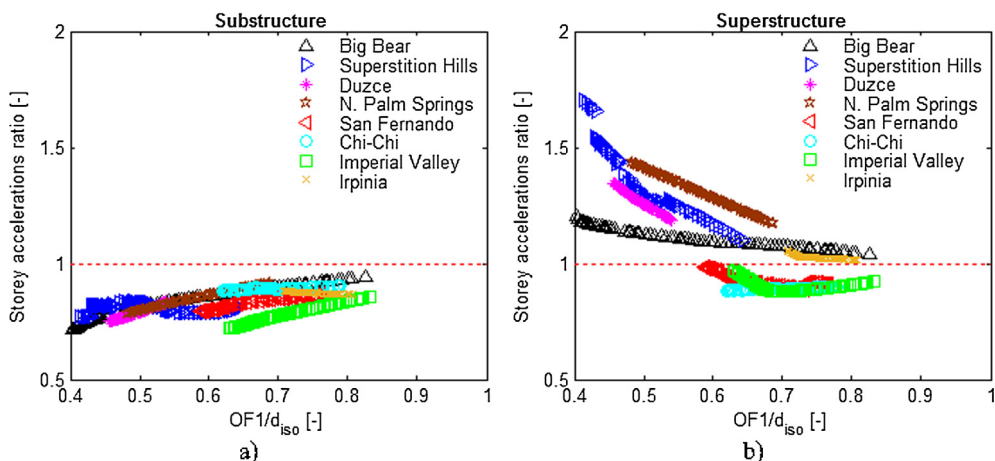


Fig. 15. For all earthquakes examined: ratio between maximum floor accelerations, with and without FVD, for (a) substructure and (b) superstructure, versus drift reduction of isolators.

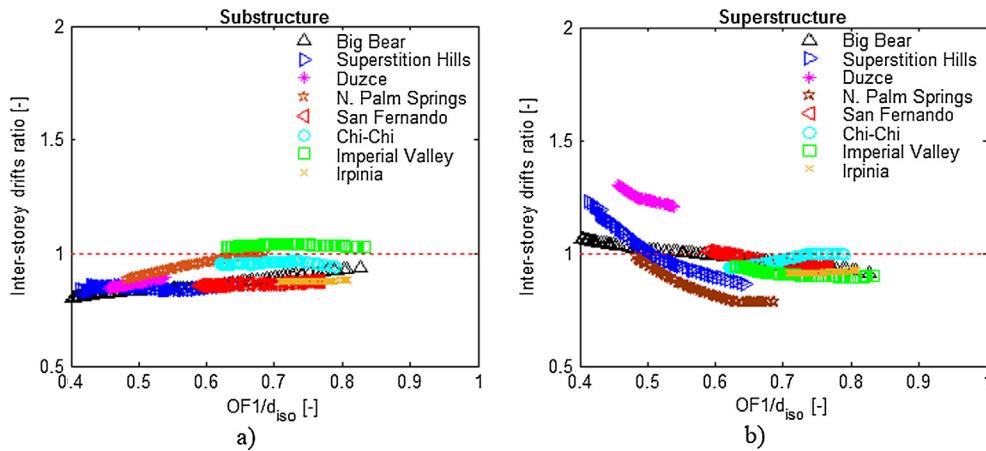


Fig. 16. For all earthquakes examined: ratio between maximum inter-storey drifts, with and without FVD, for (a) substructure and (b) superstructure, versus drift reduction of isolators.

approximately 10% to 20%, being dependent on the maximum deflection achieved by the isolation layer.

Lastly, Fig. 20 shows the additional damping ratios $\Delta\zeta_i$, estimated with complex modal analysis, provided by isolation system and dampers (case $OF_{1,min}$) to the principal modes i of the overall structure. It is interesting to note how the $\Delta\zeta$ provided by the isolators acts particularly on modes 1 and 4, whereas $\Delta\zeta$ due to the FVD acts on modes 1 and 3. This may be explained by recalling that mode 4 has a deformation of the isolation layer and a participation factor which are greater than those of mode 3: indeed, if the isolators contribute to mode 4 more than to mode 3, the optimal FVD must minimise its contribution to mode 4 (the most important higher mode), in order to contain the detrimental effects of $\Delta\zeta$ on higher modes.

The need to limit the amount of supplementary damping, to contain the excitation of the higher modes of the overall structure and consequently the inter-storey drifts and floor accelerations of the superstructure, is clear in Fig. 21, which shows the elastic displacement response spectra of mass m_3 (above the isolation layer) calculated from its absolute accelerations ($\ddot{x}_3(t) + \ddot{u}_g(t)$), for cases without and with FVD ($OF_{1,max}$ and $OF_{1,min}$) for two earthquakes. These spectra can be used to estimate the maximum displacements, relative to the isolation layer, of the superstructure modes (see Table 7), because the superstructure may be viewed as a fixed building above the isolation system. The main considerations are listed below.

Table 7

Modal frequencies f of overall structure and fixed-base superstructure, from eigenvalue analysis.

| f (mode) [Hz] | | f (1st) | f (2nd) | f (3rd) | f (4th) |
|-------------------|--------------------------|-----------|-----------|-----------|-----------|
| Overall structure | Isolation stiffness: k | 0.70 | 2.22 | 3.82 | 4.24 |
| | rk | 0.32 | 2.04 | 3.82 | 3.87 |
| Superstructure: | | 1.22 | 3.33 | 4.76 | 5.88 |

- The modal periods of the overall structure match the spectral excitations, demonstrating the accuracy of the calculations.
- The spectral displacement corresponding to the first period of vibration of the superstructure, is compatible with total drift OF_2 obtained from the THA (see Fig. 5).
- The case with maximum additional damping ($OF_{1,min}$) is associated with the greatest excitation of the superstructure modes, particularly evident for the higher modes.

6. Discussion: design consequences of research findings

The results reported above, besides demonstrating the effectiveness of optimal FVDs for improved seismic performance of inter-storey isolated buildings, show the close link of optimal α on the non-linear seismic response of the structure, and therefore on the earthquake excitation (unknown at the design stage). Therefore, although a two-dimensional optimization algorithm must be used to solve the

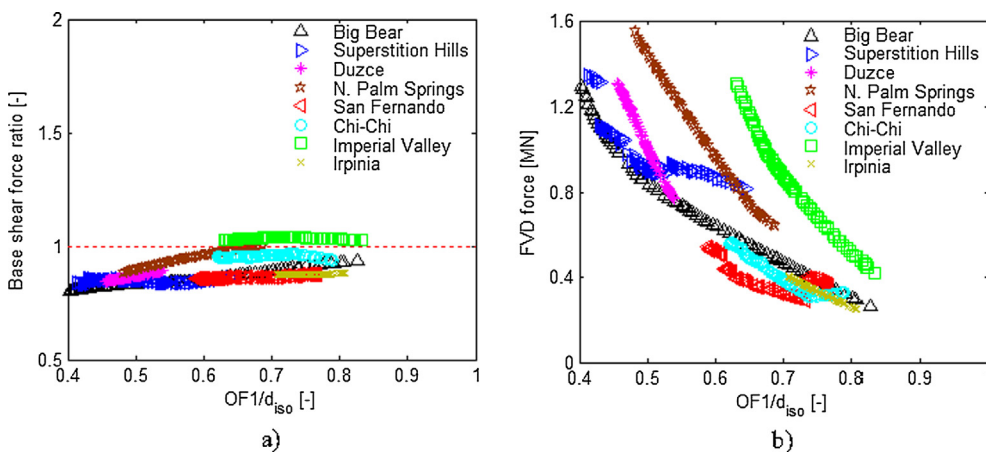


Fig. 17. For all earthquakes examined: (a) ratio between maximum base shear forces, with and without FVD, and (b) maximum FVD force, versus drift reduction of isolators.

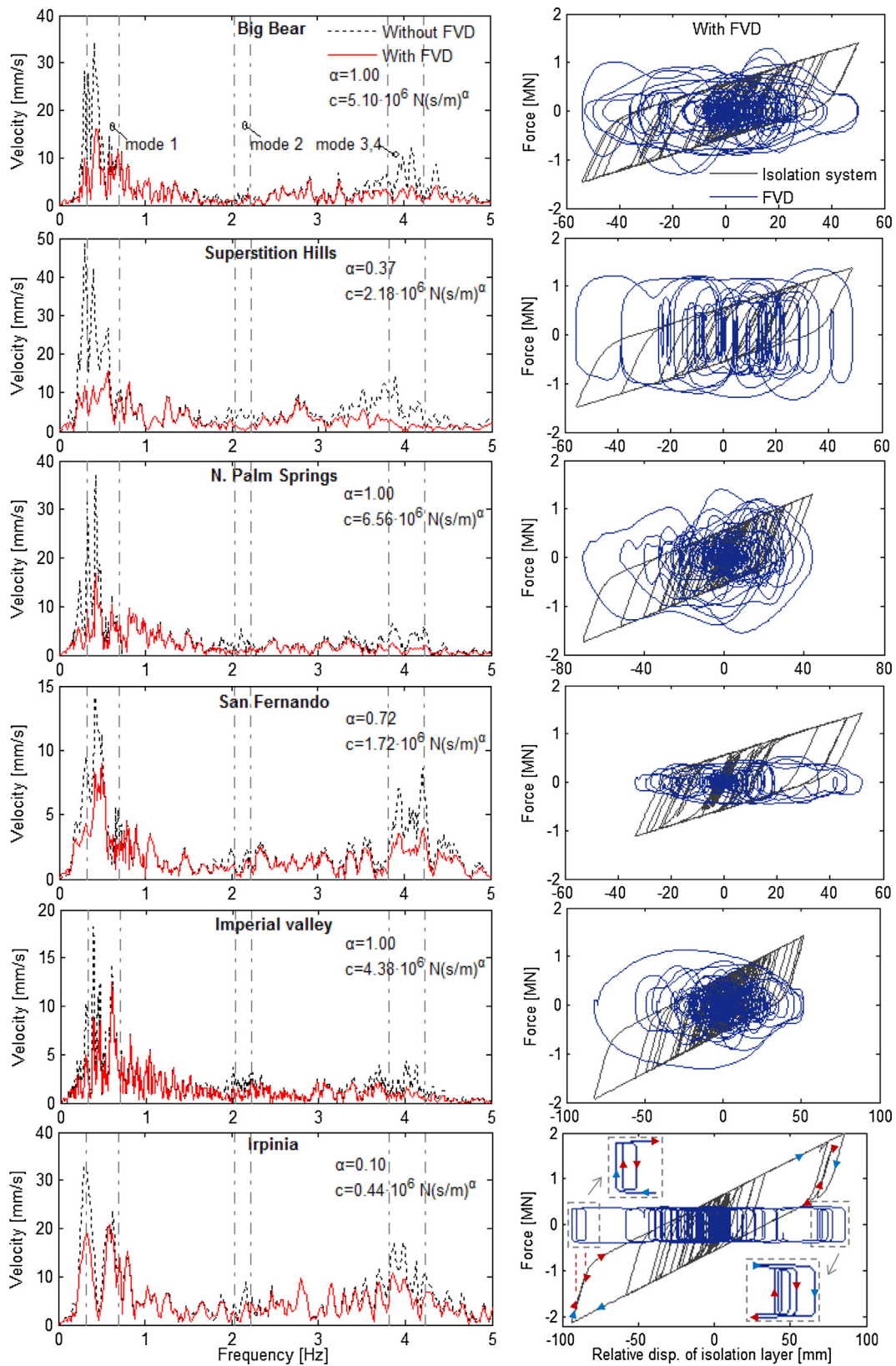


Fig. 18. Left: FFTs of relative velocity signal of isolation layer for cases without and with FVD ($OF_{T,min}$). Right: force-displacement loops in case with FVD, shown separately for isolation system and FVD.

optimization problem, its ‘direct’ application to each earthquake, which is the simplest design approach, does not seem to be sufficient to indicate the best design solution, as it may provide very different α values which cannot be averaged.

The choice of earthquakes with frequency contents more similar to each other (i.e., from the same seismic zone) and of a linear isolation system instead of the non-linear one examined in this study, may lead to simpler and more generalisable results regarding optimal α .

Table 8

Linear viscous damping coefficients c_{Eq} , for both isolators and FVD (cases $OF_{1,max}$ and $OF_{1,min}$), respectively equivalent to their non-linear energy dissipation in terms of isolator drift reduction (OF_I).

| Earthquake | $c_{Eq, Isolators}$ [Ns/m-10 ⁶] | $c_{Eq, FVD-OF_{1,max}}$ [Ns/m-10 ⁶] | $c_{Eq, FVD-OF_{1,min}}$ [Ns/m-10 ⁶] |
|--------------------|---|--|--|
| Big Bear | 1.58 | 0.79 | 5.10 |
| Superstition Hills | 2.73 | 3.68 | 9.20 |
| Duzce | 4.07 | 5.20 | 7.52 |
| North Palm Springs | 1.90 | 2.26 | 6.56 |
| San Fernando | 2.99 | 1.59 | 3.30 |
| Chi-Chi | 2.43 | 3.01 | 3.80 |
| Imperial Valley | 2.72 | 1.21 | 4.38 |
| Irpinia | 3.31 | 1.20 | 2.25 |

Nevertheless, uncertainties regarding the definition of the seismic input are significant, and the design of an isolation system must also take into account its function of lateral restraint (sufficient elastic stiffness) under non-seismic lateral service loads which, in the case of isolators with perfectly linear behaviour, should be provided by other devices.

In view of the above, some alternative solutions, proposed below, aim at providing answers to practical design needs regarding the choice of the best FVD system.

6.1. Optimal design of linear FVDs

This solution exploits the possibility of averaging the optimal values of c for the various earthquakes, to the detriment of less good structural performance when the optimal FVD is non-linear.

Figs. 22 and 23 compare the structural performance obtained with the above-determined non-linear optimal FVDs with that calculated by using optimal linear FVDs; the latter dampers were obtained by setting α at 1 and optimizing only c (on the basis of the same objective functions OF_1 and OF_2). In particular, Fig. 22 compares all the optimal solutions of linear and non-linear FVDs in terms of the drift reduction of isolators (OF_I/d_{iso}) and superstructure (OF_2/d_{sup}); Fig. 23 shows the ratio between the maximum values, obtained with linear and non-linear FVDs in the case $OF_{1,min}$, of several parameters: isolator drift, inter-storey drift and floor acceleration of both substructure and superstructure, and damper force. In the case of the optimal linear damper:

- the maximum drift of isolation layer $OF_{I,min}$ (Fig. 23(a)) obviously increases with decreasing α of the related non-linear FVD, but not excessively (up to 30%);
- the maximum floor acceleration and inter-storey drift of both substructure and superstructure (Fig. 23(b)) are not very different from those of the case with non-linear FVD (from -15% to 10%);

Table 9

First mode damping ratios in case without FVD, $\zeta_{1,without}$, and additional damping ratios provided by FVD, $\Delta\zeta_{1,FVD}$ (for both cases $OF_{1,max}$ and $OF_{1,min}$), from complex modal analysis and spectral method.

| Earthquake | Isolator drift reduction [%] (case $OF_{1,min}$) | First mode damping ratios | | | | | |
|--------------------|---|-----------------------------|---------------------------|----------------------|-------------------------|---------------------------|--------------|
| | | From complex modal analysis | | From spectral method | | | |
| | | $\zeta_{1,without}$ [%] | $\Delta\zeta_{1,FVD}$ [%] | | $\zeta_{1,without}$ [%] | $\Delta\zeta_{1,FVD}$ [%] | |
| | | | $OF_{1,max}$ | $OF_{1,min}$ | | $OF_{1,max}$ | $OF_{1,min}$ |
| Big Bear | -60 | 7.5 | 3.5 | 24.5 | 7.5 | 5.5 | 29 |
| Superstition Hills | -59 | 12.5 | 18 | 51.5 | 10.5 | 19.5 | 45 |
| Duzce | -54 | 19.5 | 27.5 | 42.5 | 18.5 | 29 | 42.5 |
| North Palm Springs | -52 | 9 | 10.5 | 33 | 8.5 | 13.5 | 27.5 |
| San Fernando | -41 | 14 | 7.5 | 16 | 14 | 8 | 19 |
| Chi-Chi | -38 | 11.5 | 14.5 | 18.5 | 10.5 | 9 | 17 |
| Imperial Valley | -37 | 12.5 | 5.5 | 21.5 | 10.5 | 5.5 | 16.5 |
| Irpinia | -29 | 15.5 | 5.5 | 11 | 15 | 7.5 | 13 |

- the maximum force of the damper (Fig. 23(c)), which appears to be the most greatly influenced parameter, may increase considerably (even up to 300%) compared with that of the non-linear FVD.

Despite optimal linear dampers dissipate slightly less energy, which explains the higher values of $OF_{1,min}$, this dissipation occurs with non-optimal hysteresis, which contrasts the potentially beneficial effect of less damping on structural performance (in particular, for the superstructure) and may lead to significantly increased damper forces.

According to these results and considerations, the optimal design of FVDs may be simplified by considering linear dampers as a first attempt: if the resulting structural performance meets the design expectations in terms of OF_I and the damper solution is economically feasible, based on the maximum damper force, then this design may be acceptable, even if it is not the truly optimal one.

6.2. Optimal design of FVDs by using a surrogate response model

According to the experience gained from this study, a convenient approach for design purposes consists of applying the optimization algorithm to a surrogate response model, rather than directly to the structural response for each accelerogram (as done in this study, allowing detailed assessment of the potential of the supplementary FVDs). The surrogate model consists of analytical functions of c and α (FVD parameters) which can predict the average response of the structural performance parameters (and thus OF_1, OF_2, \dots). This model can be determined by initially carrying out a series of parametric TH analyses, with appropriate combinations of c and α within their ranges of interest, and then interpolating the structural response values, averaged among the various accelerograms, with a response surface defined in the c - α plane, which defines the surrogate model for a structural performance parameter. Therefore, multi-objective optimization of the surrogate model equations (assumed to be OFs to be minimised) leads to an overall optimal solution instead of a local one, i.e., to a single Pareto front for all accelerograms analysed, and hence to the average optimal parameters of the FVD for the structure in question.

Such an approach, logically and numerically more complex, acquires scientific relevance when applied to several structural configurations rather than to a single case study, in order to provide general and simplified results to support the preliminary design of FVDs for inter-storey isolation systems. For this goal, which differs from that of the present study, a simplified three-lumped-mass structural model would seem more appropriate [41], and the isolation system to be investigated should, in the first place, be linear.

Lastly, as already stated, structural response as optimized in this study is not the only discriminating factor when choosing the best design solution, as technical feasibility (i.e., technical issues related to the

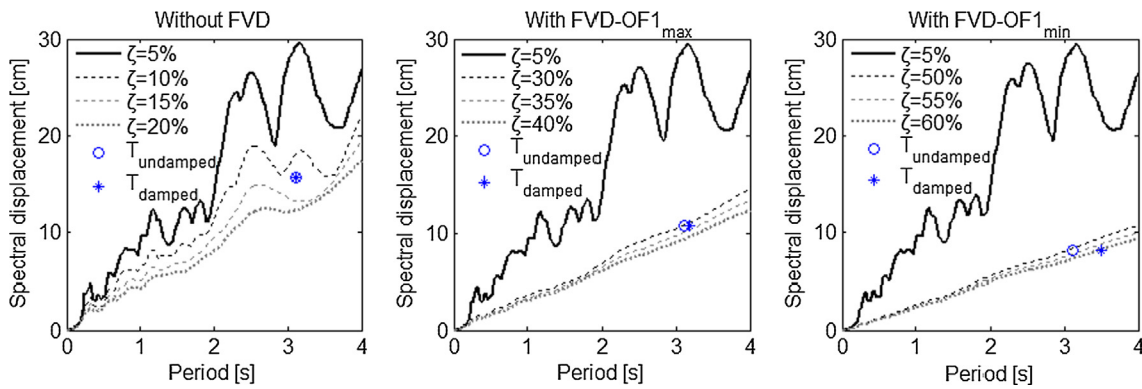


Fig. 19. North Palm Springs: application of spectral method to estimate first-mode damping ratios.

actual implementation of the isolation units combined with FVDs) and costs must also be considered. Once the most effective solutions have been identified, technical feasibility can easily be verified later; in addition, since the main aim of the extra FVD is to minimise P-Δ effects on the substructure (hence the deflection of the isolation layer), verification of isolator deformation should not be limiting; otherwise, the structural system and particularly the stiffness of the isolation layer should be redesigned more appropriately (however, this is beyond the aim of this study).

The final choice of the FVD system is certainly influenced by solution costs. In particular, to assess the economic viability of the various solutions, three components must be examined: the cost of the FVD system, which mainly depends on the maximum force and stroke of the damper, and the cost of the isolation system [42] and of the substructure, the last two being less when FVD performance improves (due to the reduction of both the deflection demand for the isolators and P-Δ effects, and thus stresses, on the substructure). This economic assessment, which would not have added scientific value to the proposed study (this being focused on a case study to evaluate in detail both the potential of the extra FVD and the dependencies of its optimal degree of linearity), should be more appropriately implemented in a parametric study like the one proposed above, which examines various structural configurations and uses a surrogate response model: in this case, the costs of the various solutions (or changes in cost compared with reference costs) may be used to define another OF to be minimised, in order to determine the best solutions from both technical and economic points of view, always with the aim of providing general results, albeit

simplified, to support the design process.

7. Conclusions

This work investigates the effectiveness of FVDs for the improved seismic performance of building structures with inter-storey isolation systems. In particular, a seven-floor building was considered as the case study, with natural and lead rubber bearings placed between the second and third floors; a multi-objective optimal design procedure (genetic algorithm NSGA-II) was applied to identify the optimal parameters (damping constants c and exponents α) of dampers which, placed inside the isolation system, allow simultaneous minimisation of isolator displacement OF_1 and total drift of the superstructure OF_2 , while performing time-history analyses with various natural records. The two objective functions (OF) are in conflict with each other, leading to the need for an optimization algorithm. Although the numerical results depend on the structural configuration of the case study, it is reasonable to believe that the potential shown by FVD systems, optimized to work together with an inter-storey isolation system, is a general result.

The main highlights are listed below.

- The supplementary damping provided by optimal FVDs allows an effective reduction (up to 60%) of the relative displacement of isolation layer OF_1 , while maintaining acceptable values for maximum inter-storey drift and floor acceleration of the superstructure. However, these values, which are slightly higher than those in the case without FVD, can be reduced if lower damper performance in

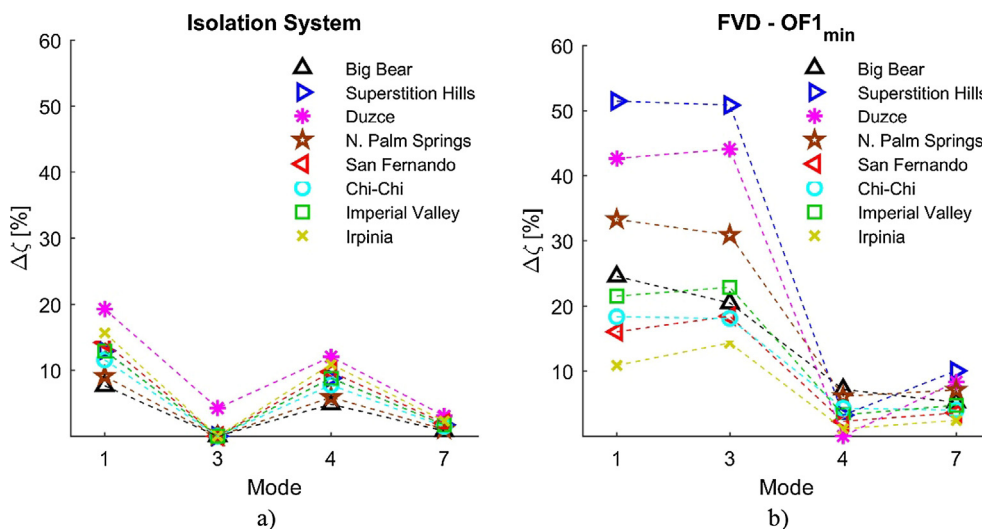


Fig. 20. Additional damping ratio $\Delta\zeta$ provided by (a) isolation system and (b) FVD (case $OF_{1,min}$), obtained from complex modal analysis for main modes of overall structure.

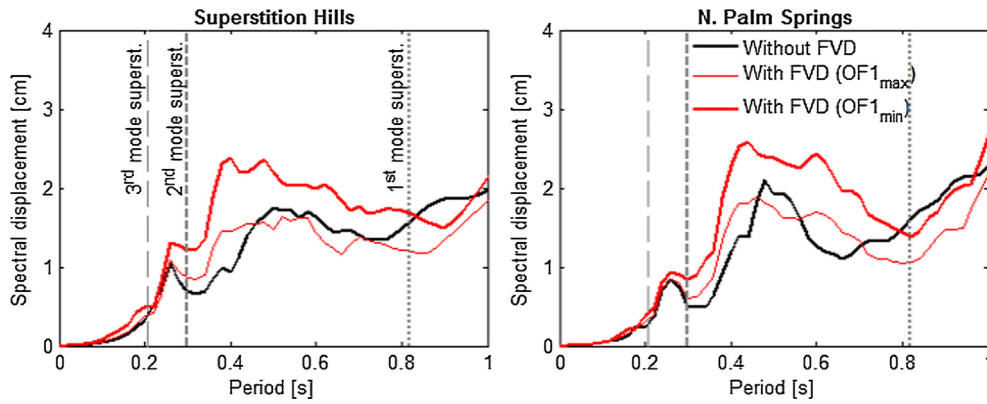


Fig. 21. Elastic displacement response spectra ($\zeta = 5\%$) of mass m_3 (above isolators), without and with FVD.

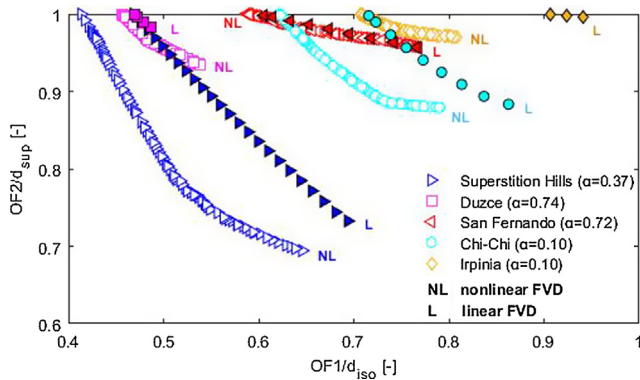


Fig. 22. Optimal solutions for OF_1 and OF_2 , for both linear and non-linear optimal FVDs, normalised to related drifts (d_{iso} , d_{sup}) obtained without FVDs.

terms of OF_1 is acceptable.

- The dynamic response of the substructure is generally improved with optimal FVDs, particularly for high supplementary damping values.
- Optimal FVDs can also effectively reduce the total base shear force by up to 20% for the highest additional damping values.
- The maximum force developed by optimal FVDs increases more than linearly with decreasing OF_1 . This may be important in choosing the best FVD, as this force is closely related to the cost of the damper.
- Damper effectiveness depends to a great extent on the non-linear

seismic response of the structure, with or without damper, since it is correlated with the values of the first mode frequencies most excited (more than one, due to the yield of the LRB isolators). Considering the case $OF_{1,min}$, the equivalent additional damping ratio, introduced by the FVD inside the structure, falls approximately in the range +10% (Irpinia earthquake) up to +50% (Superstition Hills earthquake). These values also indicate that, in some cases, FVDs may be not effective enough to justify their use.

- The optimal degree of linearity of an FVD is also strongly influenced by the non-linear seismic response of the structure - in this case, with the damper: it thus depends on the seismic input. This leads us to conclude that, for the type of structure and non-linear isolation system analysed, no value of α is more beneficial than another value based on structural data only; therefore, a two-dimensional multi-objective optimization algorithm (or a genetic algorithm such as NSGA-II) should be used. However, when the relative motion of the isolation layer with dampers tends to be dominated by a main frequency, results show that the optimal dampers tend to be linear ($\alpha = 1$), and vice versa. Since this type of motion is generally representative in the base isolation case, this evidence seems to be consistent with the results of previous experimental studies on base-isolated structures [21].
- With the aim of simplifying the design of the optimal dampers, generally non-linear, the structural performance obtained with non-linear optimal FVDs was compared with that achieved with optimal linear FVDs ($\alpha = 1$). These comparisons show that optimizing linear FVDs, computationally simpler, can still lead to reasonable design

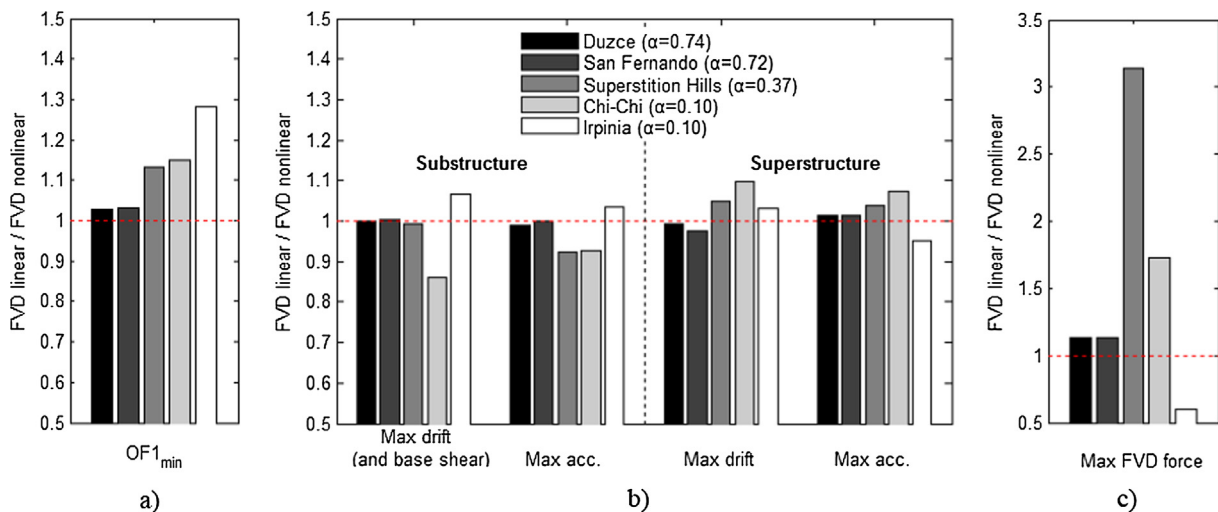


Fig. 23. Ratio between maximum values, obtained with linear and non-linear FVDs of case $OF_{1,min}$, of several parameters: (a) $OF_{1,min}$; (b) inter-storey drift and floor acceleration of substructure and superstructure; (c) damper force.

solutions (if economically feasible). In addition, if α is equal to 1, the optimal values of c for various earthquakes can be averaged, and this simplifies the identification of the overall optimal solution.

Lastly, a general discussion on the design consequences of research findings is provided.

Acknowledgments

This work was mainly funded by the Natural Science Foundation of China (no. 51778163), Cultivated Project of Outstanding Young Teachers of Guangdong Province (no. YQ2015124), Key Project of Guangzhou Municipal Universities (no. 1201610135) and National Key R&D Project of China (no. 2016YFE0127600): this funding was greatly appreciated. Thanks are due to Profs. Zhou Fu Lin, Francesca da Porto and Tan Ping for their useful advice and for creating the opportunity for Marco Donà to collaborate with the EERTC research group of the University of Guangzhou.

References

- [1] Chey M, Chase J, Mander J, Carr A. Innovative seismic retrofitting strategy of added stories isolation system. *Frontiers Struct Civil Eng* 2013;7:13–23.
- [2] Zhou FL. Seismic isolation of civil buildings in the People's Republic of China. *Prog Struct Mat Eng* 2001;3(3):268–76.
- [3] Ziyaeifar M, Noguchi T. Partial mass isolation in tall buildings. *Earthquake Eng Struct Dyn* 1998;27:49–65.
- [4] Zhang R, Phillips BM, Taniguchi S, Ikenaga M, Ikago K. Shake table real-time hybrid simulation techniques for the performance evaluation of buildings with inter-story isolation. *Struct Control Health Monitoring* 2016. <http://dx.doi.org/10.1002/stc.1971>.
- [5] Tasaka M, Mori N, Yamamoto H, Murakami K, Sueoka T. Applying seismic isolation to buildings in Japan - Retrofitting and middle-story isolation. In: Proceedings of the 18th analysis and computation specialty conference, ASCE structures congress, Vancouver, BC, Canada; 2008.
- [6] Zhou FL, Yang Z, Liu WG, Tan P. New seismic isolation system for irregular structure with the largest isolation building area in the world. In: Proceedings of the 13th world conference on earthquake engineering, Vancouver, BC, Canada; 2004.
- [7] Loh CH, Weng JH, Chen CH, Lu KC. System identification of mid-story isolation building using both ambient and earthquake response data. *Struct Control Health Monit* 2013;20:139–55.
- [8] Reggio A, De Angelis M. Optimal energy-based seismic design of non-conventional Tuned Mass Damper (TMD) implemented via inter-story isolation. *Earthquake Eng Struct Dyn* 2015;44:1623–42.
- [9] Koh CG, Balendra T. Seismic response of base isolated buildings including P-delta effects of isolation bearings. *Earthquake Eng Struct Dyn* 1989;18(4):461–73.
- [10] Makris N. Rigidity–plasticity–viscosity: can electro-rheological dampers protect base-isolated structures from near-source ground motions. *Earthquake Eng Struct Dyn* 1997;26:571–91.
- [11] Makris N, Chang S. Effects of damping mechanisms on the response of seismically isolated structures. PEER report 1998/06, Pacific Earthquake Engineering Research Center, College of Engineering, University of California, Berkeley, CA; 1998.
- [12] Kelly JM. Role of damping in seismic isolation. *Earthquake Eng Struct Dyn* 1999;28:3–20.
- [13] Discussion Hall J. The role of damping in seismic isolation. *Earthquake Eng Struct Dyn* 1999;28:1717–20.
- [14] Hall JF, Ryan KL. Isolated buildings and the 1997 UBC near-source factors. *Earthquake Spectra* 2000;16(2):393–411.
- [15] Jangid RS, Kelly JM. Base isolation for near-fault motions. *Earthquake Eng Struct Dyn* 2001;30:691–707.
- [16] Alhan C, Gavin H. A parametric study of linear and non-linear passively damped seismic isolation systems for buildings. *Eng Struct* 2004;26(4):485–97.
- [17] Politopoulos I. A review of adverse effects of damping in seismic isolation. *Earthquake Eng Struct Dyn* 2008;37:447–65.
- [18] Providakis CP. Effect of LRB isolators and supplemented viscous dampers on seismic isolated buildings under near fault excitations. *Eng Struct* 2008;32:1187–98.
- [19] Providakis CP. Effect of supplemental damping on LRB and FPS seismic isolators under near-fault ground motions. *Soil Dyn Earthquake Eng* 2009;29:80–90.
- [20] Fathi M, Makhdoumi A, Parvizi M. Effect of supplemental damping on seismic response of base isolated frames under near & far field accelerations. *KSCE J Civ Eng* 2015;19(5):1359–65.
- [21] Wolff ED, Ipek C, Constantinou MC, Tapan M. Effect of viscous damping devices on the response of seismically isolated structures. *Earthquake Eng Struct Dyn* 2015;44:185–98.
- [22] Lin WH, Chopra AK. Earthquake response of elastic SDF systems with non-linear fluid viscous dampers. *Earthquake Eng Struct Dyn* 2002;31(9):1623–42.
- [23] Tubaldi E, Ragni L, Dall'Asta A. Probabilistic seismic response assessment of linear systems equipped with nonlinear viscous dampers. *Earthquake Eng Struct Dyn* 2015;44(1):101–20.
- [24] Charmpis DC, Komodromos P, Phocas MC. Optimized earthquake response of multi-storey buildings with seismic isolation at various elevations. *Earthquake Eng Struct Dyn* 2012;41:2289–310.
- [25] Charmpis DC, Phocas MC, Komodromos P. Optimized retrofit of multi-storey buildings using seismic isolation at various elevations: assessment for several earthquake excitations. *Bull Earthq Eng* 2015;13:2745–68.
- [26] Zhou Q, Singh MP, Huang XY. Model reduction and optimal parameters of mid-story isolation systems. *Eng Struct* 2016;124:36–48.
- [27] Leu LJ, Chang JT. Optimal allocation of non-linear viscous dampers for three-dimensional building structures. *Procedia Eng* 2011;14:2489–97.
- [28] Cheng S, Darivandi N, Ghrib F. The design of an optimal viscous damper for a bridge stay cable using energy-based approach. *J Sound Vib* 2010;329:4689–704.
- [29] Cu VH, Han B, Nguyen TN. Optimal parameters of viscous damper for hanged cables in arch bridges. *KSCE J Civ Eng* 2016;20(2):847–54.
- [30] Xie Y, Zhang J. Optimal design of seismic protective devices for highway bridges using performance-based methodology and multiobjective genetic optimization. *J Bridge Eng* 2017;22(3):04016129.
- [31] Deb K, Pratap A, Agarwal S, Meyarivan T. A fast and elitist multiobjective genetic algorithm: NSGA-II. *IEEE Trans Evol Comput* 2002;6(2):182–97.
- [32] Ryan KL, Polanco J. Problems with Rayleigh damping in base-isolated buildings. *J Struct Eng* 2008;134(11):1780–4.
- [33] Pant DR, Wijeyewickrema AC, ElGawady MA. Appropriate viscous damping for nonlinear time-history analysis of base-isolated reinforced concrete buildings. *Earthquake Eng Struct Dyn* 2013;42(15):2321–39.
- [34] Ismail M, Ikhouane F, Rodellar J. The hysteresis Bouc-Wen model: A survey. *Arch Comput Methods Eng* 2009;16(02):161–88.
- [35] Ikhouane F, Hurtado JE, Rodellar J. Variation of the hysteresis loop with the Bouc-Wen model parameters. *Nonlinear Dyn* 2007;48(4):361–80.
- [36] Kalpakidis IV, Constantinou MC. Effects of heating and load history on the behaviour of lead–rubber bearings. Technical Report MCEER-08-0027, University at Buffalo, State University of New York, Buffalo, NY; 2008.
- [37] Pacific Earthquake Engineering Research Center (PEER). Strong ground motion database; 2012. (Available from: <http://peer.berkeley.edu/>), [December 3, 2012].
- [38] Coello Coello C, Lamont GB, Van Veldhuizen DA. Evolutionary algorithms for solving multi-objective problems. Genetic and Evolutionary Computation Series 2007. Series Editors: Goldberg DE, Koza JR. Springer Science + Business Media, LLC. ISBN 978-0-387-33254-3.
- [39] Donà M, Muhr AH, Tecchio G, da Porto F. Experimental characterization, design and modelling of the RBRL seismic-isolation system for lightweight structures. *Earthquake Eng Struct Dyn* 2017;46:831–53.
- [40] Donà M. Rolling-Ball Rubber-Layer system for the lightweight structures seismic protection: experimentation and numerical analyses. Ph.D. Thesis. University of Trento, Department DICAM, Italy; 2015.
- [41] Wang SJ, Chang KC, Hwang JS, Lee BH. Simplified analysis of mid-storey seismically isolated buildings. *Earthquake Eng Struct Dyn* 2011;40:119–33.
- [42] Manos GC, Mitoulis SA, Sextos AG. A knowledge-based software for the preliminary design of seismically isolated bridges. *Bull Earthq Eng* 2012;10:1029–47.